nature physics

ARTICLES

PUBLISHED ONLINE: 12 DECEMBER 2016 | DOI: 10.1038/NPHYS3984

Growth and division of active droplets provides a model for protocells

David Zwicker[1,2†], Rabea Seyboldt[1†], Christoph A. Weber[1], Anthony A. Hyman[3] and Frank Jülicher[1*]

It has been proposed that during the early steps in the origin of life, small droplets could have formed via the segregation of molecules from complex mixtures by phase separation. These droplets could have provided chemical reaction centres. However, whether these droplets could divide and propagate is unclear. Here we examine the behaviour of droplets in systems that are maintained away from thermodynamic equilibrium by an external supply of energy. In these systems, droplets grow by the addition of droplet material generated by chemical reactions. Surprisingly, we find that chemically driven droplet growth can lead to shape instabilities that trigger the division of droplets into two smaller daughters. Therefore, chemically active droplets can exhibit cycles of growth and division that resemble the proliferation of living cells. Dividing active droplets could serve as a model for prebiotic protocells, where chemical reactions in the droplet play the role of a prebiotic metabolism.

Living systems consist of cells that can grow and divide. Cells take up matter from the outside world to grow, they release waste products, and they are able to divide, creating more cells. A fundamental question is to understand how cells arose early in evolution. Early in the origin of life, chemical reaction centres or chemical microreactors had to form to organize chemical reactions in space. These microreactors had to exchange material with the outside and they had to propagate. Recently, the idea of Oparin and Haldane[1,2] that small droplets, which they called coacervates, could organize molecules in microreactors has resurfaced to prominence[3–8]. Such droplets are liquid-like aggregates that concentrate molecules that have separated from a complex mixture.

Liquid droplets are self-organized structures that coexist with a surrounding fluid[7,9]. The interface separating the two coexisting phases provides them with a well-defined surface. The associated surface tension forces them into a spherical shape. Furthermore, many substances can diffuse across the interface. The segregation of components into a droplet concentrates material in a confined volume, which may facilitate specific chemical reactions. Thus, droplets provide containers in which chemical reactions can be spatially organized. Although the thermodynamics of phase transitions can explain how liquid drops can form, it is unclear how such droplets could propagate by division and subsequent growth, an ability that would be key at the origin of life.

Droplets grow by taking up material from a supersaturated environment or by Ostwald ripening[9–13]. Ostwald ripening describes the exchange of material between droplets by diffusion, usually leading to growth of large droplets while small droplets shrink. Furthermore, droplets can increase in size by fusion of two droplets into a larger one. These processes lead to the formation of droplets of increasing size while the droplet number decreases with time. This behaviour is opposite to that of cells, which have a characteristic size and increase their number by division. How could droplets divide and propagate?

We have recently shown that droplets that are maintained away from thermodynamic equilibrium by a chemical fuel can have unusual properties[14,15]. In particular, in the presence of chemical reactions, Ostwald ripening can be suppressed[15] and multiple droplets can stably coexist, with a characteristic size set by the reaction rates[15–18]. Here, we show that, surprisingly, spherical droplets subject to chemical reactions spontaneously split in two smaller daughter droplets of equal size. Therefore, chemically active droplets can grow and subsequently divide and thereby propagate by using up the inflowing material as a fuel. We conclude that droplets can indeed behave similarly to cells in the presence of chemical reactions that are driven by an external fuel reservoir. Such active droplets could represent models for growing and dividing protocells with a rudimentary metabolism that is represented by simple chemical reactions that are maintained by an external fuel.

Division of active droplets

Droplets can serve as small compartments to spatially organize chemical reactions. The emergence of droplets requires phase separation into two coexisting liquid phases of different composition. Phase separation is driven by molecular interactions, where molecules with an affinity for each other lower their energy if they come closely together. A fluid can demix if the energy decrease associated with molecular interactions overcomes the effects of entropy increase by mixing[19,20]. If those interactions are strong, a sharp interface separates the coexisting phases.

Droplets can become chemically active if the material of the droplet is produced and destroyed by chemical reactions. An example that resembles a simple protocell is shown schematically in Fig. 1a. The droplet is formed by a droplet material D that is generated inside the droplet from a high-energy precursor N, which plays the role of a nutrient. Droplet material can degrade into a lower energy component W that plays the role of a waste, which leaves the droplet by diffusion. The droplet can survive if N is continuously supplied and W is continuously removed. This can be achieved by recycling N using an external energy source such as a fuel or radiation.

Inspired by Oparin[21], we discuss the physics of such active droplets using a simple model with only two components A and B (see Fig. 1b). The droplet material B phase separates from

[1]Max Planck Institute for the Physics of Complex Systems, 01187 Dresden, Germany. [2]School of Engineering and Applied Sciences, Harvard University, Cambridge, Massachusetts 02138, USA. [3]Max Planck Institute of Molecular Cell Biology and Genetics, 01307 Dresden, Germany. †These authors contributed equally to this work. *e-mail: julicher@pks.mpg.de

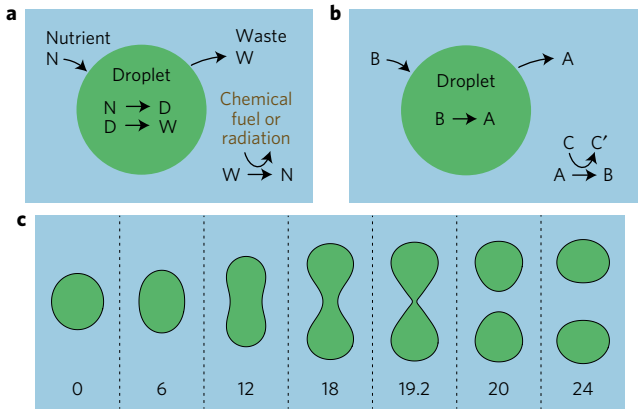

Figure 1 | Division of chemically active droplets. a, Schematic representation of an active droplet as a simple model of a protocell. The droplet (green) consists of a droplet material D. Nutrients N of high chemical energy can diffuse into the droplet. Inside the droplet, N is transformed to D by chemical reactions. Droplet material D is degraded chemically into low-energy waste W that leaves the droplet. **b**, Simple model, with droplet material B and soluble component A. The system is driven by a chemical fuel C that is transformed to the reaction product C′. **c**, Sequence of shapes of a dividing droplet at different times as indicated. The dynamic equations of a continuum model corresponding to the situation shown in **b** were solved numerically. The droplet shapes are shown as equal concentration contours (black). Parameter values are $\nu_- t_0/\Delta c = 7\times10^{-3}$, $\nu_+ t_0/\Delta c = 1.9\times10^{-3}$, and $k_\pm t_0 = 10^{-2}$, where t_0 is a characteristic time of the continuum model (see Supplementary Information). Indicated times are given in units of $10^2\, t_0$.

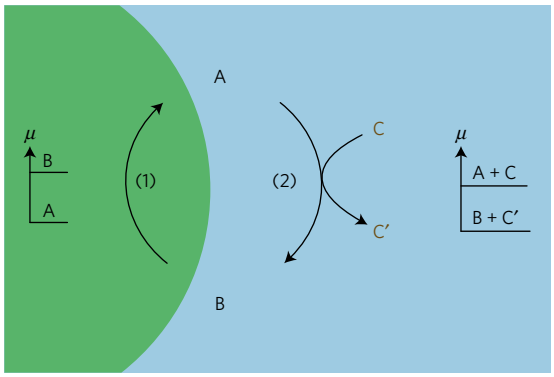

Figure 2 | Reaction rates and energy supply. Schematic representation of the reaction cycle involving the two pathways (1) and (2). The differences of the chemical potentials μ determine the direction of the spontaneous reactions: coupling to the chemical fuel C with reaction product C′ drives reaction pathway (2) in the direction A → B outside the droplet. Inside the droplet, where the concentration of C is smaller, reaction pathway (1) in the direction B → A dominates. See Methods and the Supplementary Information for details.

the solvent. It can spontaneously be degraded by a chemical reaction

$$\mathrm{B} \rightarrow \mathrm{A} \qquad (1)$$

into molecules of type A that are soluble in the background fluid and leave the droplet. The backward reaction A → B is not proceeding spontaneously because B is of higher energy than A. New droplet material B can be produced by the second reaction

$$\mathrm{A} + \mathrm{C} \rightarrow \mathrm{B} + \mathrm{C}' \qquad (2)$$

that is coupled to a fuel C. Here C′ is the low-energy reaction product of the fuel molecules. The chemical potential difference $\Delta\mu_\mathrm{C} = \mu_\mathrm{C} - \mu_{\mathrm{C}'} > 0$ provided by the fuel powers the production of high-energy B from low-energy A. The difference $\Delta\mu_\mathrm{C}$ can be maintained constant if the concentrations of C and C′ are set by an external reservoir. In this case, the system is kept away from a thermodynamic equilibrium (see Fig. 2 and Methods).

The combination of phase separation and non-equilibrium chemical reactions can be studied in a continuum model[15–17] (see Supplementary Information). Using this model, we find that spherical droplets that are chemically active can undergo a shape instability and split into two smaller droplets, despite their surface tension (see Fig. 1c and Supplementary Movie). A droplet first grows until it reaches its stationary size[15]. Then, the droplet starts to elongate and forms a dumbbell shape. This dumbbell splits into two smaller droplets of equal size. The resulting smaller droplets grow again until a new division may occur, reminiscent of living cells.

To investigate the stability of spherical droplets, we study the droplet shape by an effective droplet model (see Fig. 3 and Methods). Figure 4a shows the behaviour of the stationary droplet radius in this model as a function of the supersaturation ϵ. This supersaturation is the excess concentration of droplet material far from the droplet, generated by the chemical reaction (2). For $\epsilon > 0$, material diffuses to the droplet and is incorporated. Figure 4a shows that for a given turnover ν_- of droplet material inside the droplet (see Methods), stationary droplets exist only for sufficiently large supersaturation. Beyond this threshold, droplets smaller than the critical radius (Fig. 4a, black dotted lines) shrink, while larger droplets grow toward the stationary radius (Fig. 4a, black solid line)[15]. At this stationary radius, the influx of B due to the supersaturation outside is balanced by the efflux of material A produced inside the droplet. Thus, a larger turnover leads to smaller droplets (Fig. 4a).

Droplet division occurs when a spherical droplet becomes unstable and elongates. We performed a linear stability analysis of spherical droplets at their stationary radius in the effective droplet model (see Supplementary Methods). We find that for increasing supersaturation ϵ, a spherical droplet with surface tension undergoes a shape instability when its radius reaches a critical value R_div that depends on the reaction rates and droplet parameters (see Fig. 4a). Beyond the radius R_div, the spherical shape is unstable and any small shape deformation triggers the elongation of the droplet shape along one axis.

The stability analysis of the effective droplet model can be represented in a state diagram (see Fig. 4b). We find three different regions as a function of supersaturation ϵ and turnover of droplet material ν_-. A region where droplets do not exist (white), a region in which spherical droplets are stable (blue), and a region in which spherical droplets are unstable (red).

To study how the shape instability leads to droplet division, we investigated the droplet dynamics beyond the linearized analysis using the continuum model. This model can capture the topological changes of the droplet surface that occur during division. Numerical calculations of the continuum model (see Supplementary Information) confirm the results of the stability analysis. An example of droplet division is shown in Fig. 1c. The state diagram for the continuum model is shown in Fig. 4c. Comparing the state diagrams Fig. 4b and Fig. 4c reveals that both models exhibit qualitatively the same behaviours. Note that due to simplifications in the effective droplet model, the parameters are different in both models (see Supplementary Information) and the regions in both diagrams differ slightly. While Fig. 4b shows only where droplets become unstable (red line), Fig. 4c reveals the behaviours of droplets in the unstable region. We find that droplets typically divide into two daughters (red circles). However, for some

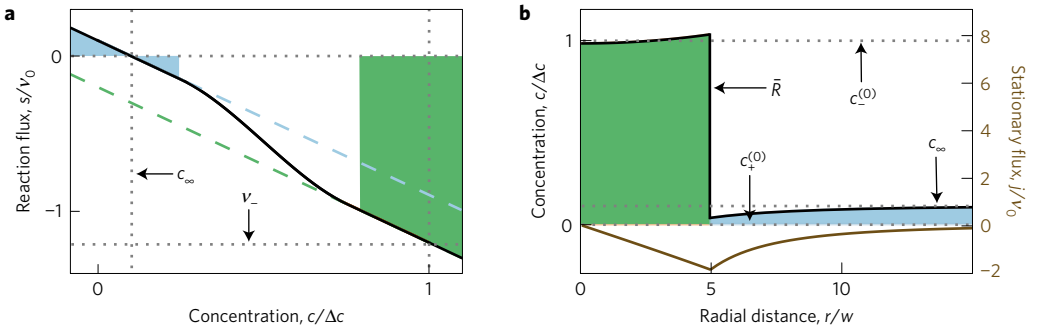

Figure 3 | Reaction flux, concentration profile and diffusion flux in an effective droplet model. Shaded regions correspond to concentration ranges inside (green) and outside the droplet (blue). **a**, Chemical reaction flux s as a function of concentration (black). The linearized fluxes inside (green) and outside the droplet (blue) are indicated as dashed lines. **b**, Stationary concentration profile of the droplet material B (black) and stationary flux $j=-D_\pm\partial_r c$ (brown, axis on the right). The droplet radius $\bar{R}$, the equilibrium concentrations $c_\pm^{(0)}$, and the concentration far from the droplet c_∞ are indicated. The corresponding supersaturation is defined as $\epsilon=(c_\infty-c_+^{(0)})/\Delta c$ (see Methods). Parameter values are: $k_\pm\tau_0=10^{-2}$, $c_+^{(0)}=0$, $\beta_-=\beta_+$, $D_-=D_+$, $\nu_0=10^{-2}\Delta c/\tau_0$, $\nu_-/\nu_0=1.2$ and $\nu_+/\nu_0=0.1$.

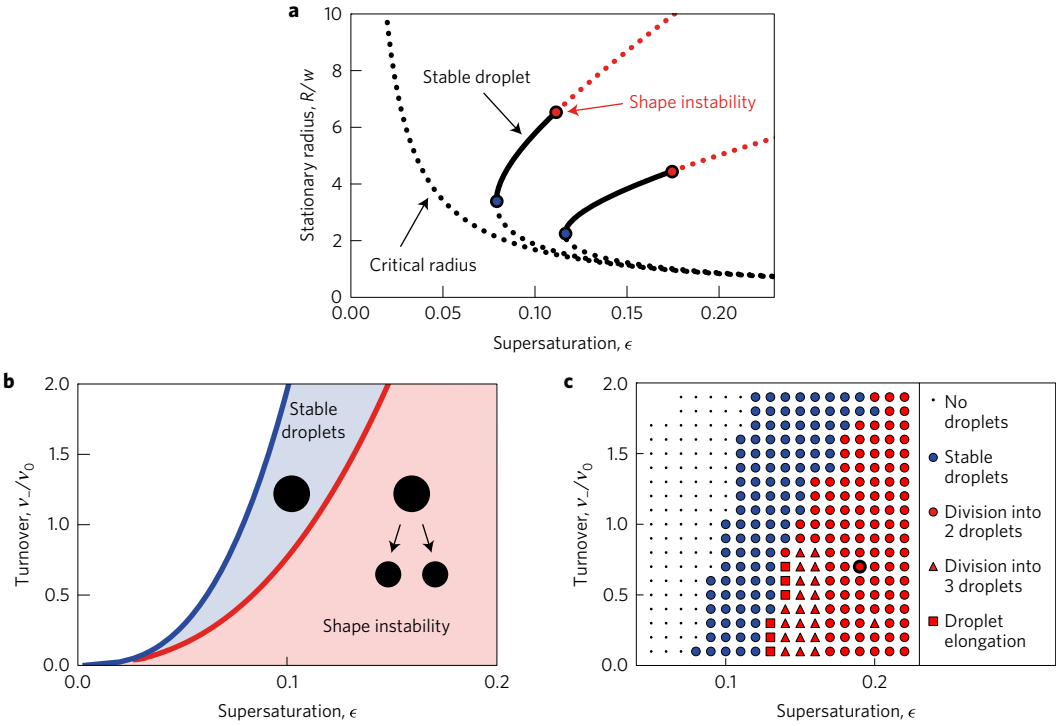

Figure 4 | Stationary droplet radii and stability diagrams. a, Stationary radii of active droplets. The droplet radius R of spherical droplets is shown as a function of supersaturation ϵ for different values of normalized turnover $\nu_-/\nu_0=0,1,3$ (from left to right). Radii of stable droplets are shown as solid black lines. Dotted lines indicate states where droplets are unstable with respect to size (black) or shape (red). The results are obtained for the effective droplet model described in the Methods. Parameter values are: $k_\pm\tau_0=10^{-2}$, $c_+^{(0)}=0$, $\beta_-=\beta_+$, $D_-=D_+$ and $\nu_0=10^{-2}\Delta c/\tau_0$. Here, $w=6\beta_+\gamma/\Delta c$, and $\tau_0=w^2/D_+$ are characteristic length and time scales. **b**, Stability diagram of active droplets as a function of supersaturation $\epsilon=\nu_+/(k_+\Delta c)$ and turnover ν_- of droplet material. Droplets either dissolve and disappear (white region), are spherical and stable (blue region), or undergo a shape instability and typically divide (red region). The lines of instability are obtained for the droplet model described in the Methods for the same parameters as in **a**. **c**, The same stability diagram as in **b** but for the continuum model described in the Supplementary Information. The behaviour of droplets is indicated by symbols for different values of ν_- and ϵ. Parameter values are $k_\pm t_0=10^{-2}$ (see Supplementary Information). The parameter values corresponding to Fig. 1c are indicated (large red circle).

parameter values they divide into three droplets (red triangles). In a few cases, division was not seen during the time of calculations (red squares). In these cases droplets elongated until they reached the size of the simulation box. It is unclear whether they would divide in a larger box.

Our numerical calculations also reveal that droplets typically undergo multiple divisions (see Fig. 5a and Supplementary Movie). After a first division, the smaller daughters grow until they divide again when they reach the radius $R_{\rm div}$. Interestingly, the division axes are not independent of each other (see Fig. 5a). In the absence of system boundaries, the division axes of both daughters are perpendicular to the first division axis (see Fig. 5b). Similarly, when the four granddaughters divide, their division axes are perpendicular to both the division axes of the first and the second division. The division axes in subsequent droplet divisions are determined by droplet interactions via the concentration fields surrounding the droplets. The two growing daughter droplets effectively compete for droplet material, leading

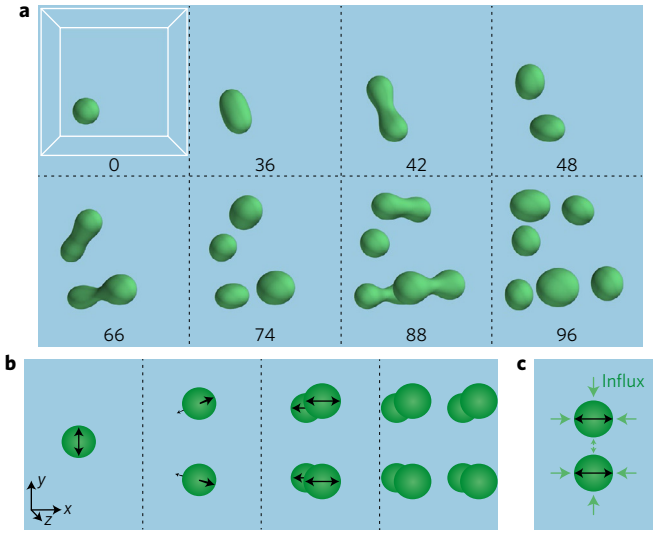

Figure 5 | Cycles of growth and divisions. a, Sequence of droplet divisions at different times as indicated in units of $10^2 t_0$. Droplet configurations obtained from numerical solutions to the continuum model are represented as three-dimensional shapes. Parameter $\nu_+ t_0/\Delta c = 2 \times 10^{-3}$. Remaining parameters are the same as in Fig. 1c. **b**, Schematic representation of the orientation of subsequent division axes. **c**, Droplet division is oriented along the axis for which diffusion fluxes (green arrows) are maximal.

to the depletion of droplet material in the space between them. Therefore, diffusion fluxes and growth rates are larger along axes perpendicular to the previous division axis (see Fig. 5c). This bias due to droplet interactions determines the division axes. In our numerical calculations, boundary conditions also influence the droplet divisions and slightly modify the division axes (see Fig. 5a).

Could such droplet division occur in experiments and what conditions are needed? To address this question, we provide in Table 1 two examples of parameter sets for which droplets would divide. These parameters are chosen such that dividing droplets would have a diameter of several micrometres and the material in the droplet would turn over in about two minutes. In case I, the surface tension is chosen small, similar to surface tensions that can be found in colloidal droplets or protein liquid phases[3]. The interfacial width in this case is of the order of ten nanometres. Case II describes droplets with a surface tension similar to that of oil/water interfaces with an interface thickness of about one nanometre. These examples show that small droplets that could be observable under the microscope could indeed undergo droplet division for plausible rates of chemical reactions and realistic interfacial tensions. However, as shown in Supplementary Information IV, droplet division for macroscopic droplets of millimetre or centimetre size will be difficult to achieve.

Chemically active droplets as a model for protocells

In this paper we have introduced a simple model to show that chemically active droplets can undergo cycles of growth and division reminiscent of cells. Our model combines the set of features that are minimally required for droplet division: two different chemical components undergoing reactions; phase separation; external energy input that maintains the system away from thermodynamic equilibrium. Our work shows that such droplet division would be expected to occur in small droplets. It will be an important challenge to observe this droplet division in future experiments. We have provided in Table 1 examples of parameter values for which micrometre-sized droplets would divide. These parameter values could in principle be achieved in artificial droplets or in *in vitro* studies of protein droplets.

The fact that active droplets tend to become unstable and divide is an unusual behaviour of droplets because surface tension usually opposes such shape changes. An instability of the droplet shape requires non-equilibrium conditions. In our model, these non-equilibrium conditions are provided by the energy input of a chemical fuel. The resulting chemical reactions drive diffusive fluxes across characteristic length scales as known for reaction–diffusion systems[22,23]. In the presence of droplet interfaces, these fluxes can induce a shape instability of stationary droplets. In the absence of chemical reactions and the resulting fluxes, the shape instability does not occur. The shape instability leading to droplet division introduced here can be compared to the Mullins–Sekerka instability often discussed in the context of crystal growth[24] (also see Supplementary Information). Both instabilities require a diffusion flux toward the interface. In the case of the Mullins–Sekerka instability the shape of a growing aggregate becomes unstable. For example, an interface can become unstable with respect to growing spikes called dendrites beyond a critical interface velocity. In contrast, the chemical-reaction-induced shape instability discussed here can occur for a stationary, non-growing droplet. This difference is important because in the case of a Mullins–Sekerka instability, the instability of a droplet does not lead to a shrinking waistline and fission but rather to the formation of a growing dendritic structure[25]. Only for the instability of a steady-state droplet found here does the instability generate a narrowing of the waistline of the initial droplet shape leading to fission in two droplets (see Supplementary Information III).

We propose that active droplets that turn over by chemical reactions provide a simple model for prebiotic protocells. The nature of such protocells remains unknown. While evolution can be reconstructed to a large extent both from fossil records and from the phylogenetic analysis of today's genomes, the structure and nature of early life forms remain quite unclear[26]. This leads to many interesting questions. How did the first replicating cells emerge from prebiotic precursors? Since replication involves specific chemical reactions, early replicators had to spatially organize chemistry and to concentrate certain molecules to facilitate reactions that would be unlikely in dilute or disorganized situations. Therefore, protocells as containers for chemical reactions had to appear.

Alexander Oparin pioneered the idea that macromolecular aggregation could lead to the formation of 'coacervates', liquid droplets that could organize chemistry and provide microreactors in which selected molecules were concentrated for prebiotic chemistry[1,27]. What types of molecules could have formed such droplets? It is interesting to note that modern-day cells possess a number of chemical compartments that are not separated by a membrane from the cell cytoplasm but that form by phase separation from the cytoplasm[3,7,28,29]. Many of these compartments are liquid and consist of RNA molecules and RNA-binding proteins[30–33]. The RNA world hypothesis suggests that at the origin of life, RNA was both the carrier of genetic information and could have acted as early enzymes[34,35]. Folded RNA molecules called ribozymes can be catalysts for many reactions including RNA processing[36]. Combining RNA with other molecules such as simple peptides may have been sufficient to organize RNA in liquid droplets[4]. The steps from chemically active droplets to the first dividing cells with membranes pose a big challenge to the understanding of early evolution. While it has been suggested that ribozymes that replicate RNA could have formed by molecular evolution[35,37], it is unclear how a cell membrane and cell division could have emerged[38–41].

The possibility that droplets may spontaneously divide has been discussed in the context of either negative surface tension[42,43] or in active nematic droplets[44]. Here we show that simply adding a proto-metabolism to droplets formed by classical phase separation can naturally lead to droplet division despite their surface tension. Membranes or surfactants are therefore not required to achieve

Table 1 | Examples of parameter values for dividing droplets.

	$D_\pm$ ($\mu m^2\,s^{-1}$)	w (nm)	γ ($mN\,m^{-1}$)	$c_-^{(0)}$ (mM)	$c_+^{(0)}$ (mM)	ν_- ($mM\,s^{-1}$)	$l_\pm$ (mm)	ϵ	t_R (s)	R_{div} (μm)
Case I	10	10	10^{-3}	100	1	1	0.1	2×10^{-3}	100	3
Case II	10	1	10	10^3	10^{-3}	10	5	8×10^{-4}	100	1

Parameters are defined in the Methods. For these parameters, the resulting supersaturation ϵ, the turnover time $t_R = c_-^{(0)}/\nu_-$, and the radius R_{div} where the stationary droplet shape becomes unstable are given. Case I is motivated by colloidal droplets or liquid protein phases with low surface tension. For Case II we chose properties of typical water/oil droplets.

division of prebiotic cells. Active droplets are natural systems to organize the chemistry of replicators and to form protocells. Such droplets can in principle form spontaneously by a rare nucleation event. Once they exist, they grow and divide. They provide a container for chemical reactions and they concentrate selected molecules that have an affinity to the droplet phase. The liquid and dynamic nature of active droplets implies that components in the droplet can mix and chemical reactions are facilitated. Protocells formed by active droplets require a constant energy supply, which could have been provided by a chemical fuel, by tides, or by temperature gradients, for example, in hydrothermal vents on the seafloor[2,45–47]. The chemical reactions by which new droplet material is formed and subsequently degraded represent an early metabolism. It will be interesting to generalize our study to systems with many droplets of different type. This corresponds to prebiotic ecosystems in which droplets may have 'symbiotic' relationships if one produces the nutrient of the other. Alternatively one may find predator–prey relationships when a droplet fuses with a different one to harvest its resources.

The possibility that early protocells were active membraneless droplets suggests possible scenarios by which cell membranes could have appeared. The droplet surface is an interface that will in general attract certain types of amphiphilic molecule. Such molecules have an affinity neither for the droplet phase nor for the surrounding fluid. As a result, selected molecules might populate the droplet surface and surface chemical reactions could be established. If lipids were available in the outside fluid, lipid monolayers or bilayers could be attracted to the specific droplet surface chemistry. Our work shows that active droplets can naturally divide. Therefore, protocells could have obtained their membranes long after the first dividing cells had appeared on Earth.

Methods

Methods, including statements of data availability and any associated accession codes and references, are available in the online version of this paper.

Received 29 April 2016; accepted 10 November 2016; published online 12 December 2016

References

1. Oparin, A. I. *Origin of Life* (Dover, 1952).
2. Haldane, J. B. S. The origin of life. *Ration. Annu.* **148,** 3–10 (1929).
3. Brangwynne, C. P. *et al*. Germline P granules are liquid droplets that localize by controlled dissolution/condensation. *Science* **324,** 1729–1732 (2009).
4. Koga, S., Williams, D. S., Perriman, A. W. & Mann, S. Peptide-nucleotide microdroplets as a step towards a membrane-free protocell model. *Nat. Chem.* **3,** 720–724 (2011).
5. Crosby, J. *et al*. Stabilization and enhanced reactivity of actinorhodin polyketide synthase minimal complex in polymer–nucleotide coacervate droplets. *Chem. Commun.* **48,** 11832 (2012).
6. Sokolova, E. *et al*. Enhanced transcription rates in membrane-free protocells formed by coacervation of cell lysate. *Proc. Natl Acad. Sci. USA* **110,** 11692–11697 (2013).
7. Hyman, A. A., Weber, C. A. & Jülicher, F. Liquid-liquid phase separation in biology. *Annu. Rev. Cell Dev. Biol.* **30,** 39–58 (2014).
8. Tang, T.-Y. D., van Swaay, D., DeMello, A., Ross Anderson, J. L. & Mann, S. *In vitro* gene expression within membrane-free coacervate protocells. *Chem. Commun.* **51,** 11429–11432 (2015).
9. Bray, A. Theory of phase-ordering kinetics. *Adv. Phys.* **43,** 357–459 (1994).
10. Ostwald, W. Studien über die Bildung und Umwandlung fester Körper. *Z. Phys. Chem.* **22,** 289–330 (1897).
11. Lifshitz, I. M. & Slyozov, V. V. The kinetics of precipitation from supersaturated solid solutions. *J. Phys. Chem. Solids* **19,** 35–50 (1961).
12. Binder, K. & Stauffer, D. Statistical theory of nucleation, condensation and coagulation. *Adv. Phys.* **25,** 343–396 (1976).
13. Voorhees, P. W. Ostwald ripening of two-phase mixtures. *Annu. Rev. Mater. Sci.* **22,** 197–215 (1992).
14. Zwicker, D., Decker, M., Jaensch, S., Hyman, A. A. & Jülicher, F. Centrosomes are autocatalytic droplets of pericentriolar material organized by centrioles. *Proc. Natl Acad. Sci. USA* **111,** E2636–E2645 (2014).
15. Zwicker, D., Hyman, A. A. & Jülicher, F. Suppression of Ostwald ripening in active emulsions. *Phys. Rev. E* **92,** 012317 (2015).
16. Puri, S. & Frisch, H. Segregation dynamics of binary mixtures with simple chemical reactions. *J. Phys. A* **27,** 6027–6038 (1994).
17. Glotzer, S. C., Stauffer, D. & Jan, N. Monte Carlo simulations of phase separation in chemically reactive binary mixtures. *Phys. Rev. Lett.* **72,** 4109–4112 (1994).
18. Carati, D. & Lefever, R. Chemical freezing of phase separation in immiscible binary mixtures. *Phys. Rev. E* **56,** 3127–3136 (1997).
19. Huggins, M. L. Solutions of long chain compounds. *J. Chem. Phys.* **9,** 440 (1941).
20. Flory, P. I. Thermodynamics of high polymer solutions. *J. Chem. Phys.* **10,** 51–61 (1942).
21. Oparin, A. *Proiskhozhedenie Zhizni Mosckovskii Rabochii* (Reprinted and translated in JD Bernal (1967) The Origin of Life London; Weidenfeld and Nicolson, 1924).
22. Turing, A. The chemical basis of morphogenesis. *Phil. Trans. R. Soc. Lond.* **237,** 37–72 (1952).
23. Gierer, A. & Meinhardt, H. A theory of biological pattern formation. *Biol. Cybern.* **12,** 30–39 (1972).
24. Mullins, W. W. & Sekerka, R. F. Morphological stability of a particle growing by diffusion or heat flow. *J. Appl. Phys.* **34,** 323–329 (1963).
25. Langer, J. S. Instabilities and pattern formation in crystal growth. *Rev. Mod. Phys.* **52,** 1–28 (1980).
26. Woese, C. R., Kandler, O. & Wheelis, M. L. Towards a natural system of organisms: proposal for the domains Archaea, Bacteria, and Eucarya. *Proc. Natl Acad. Sci. USA* **87,** 4576–4579 (1990).
27. Fox, S. W. The evolutionary significance of phase-separated microsystems. *Orig. Life* **7,** 49–68 (1976).
28. Brangwynne, C. P. Soft active aggregates: mechanics, dynamics and self-assembly of liquid-like intracellular protein bodies. *Soft Matter* **7,** 3052–3059 (2011).
29. Toretsky, J. A. & Wright, P. E. Assemblages: functional units formed by cellular phase separation. *J. Cell Biol.* **206,** 579–588 (2014).
30. Weber, S. C. & Brangwynne, C. P. Getting RNA and protein in phase. *Cell* **149,** 1188–1191 (2012).
31. Elbaum-Garfinkle, S. *et al*. The disordered P granule protein LAF-1 drives phase separation into droplets with tunable viscosity and dynamics. *Proc. Natl Acad. Sci. USA* **112,** 7189–7194 (2015).
32. Molliex, A. *et al*. Phase separation by low complexity domains promotes stress granule assembly and drives pathological fibrillization article phase separation by low complexity domains promotes stress granule assembly and drives pathological fibrillization. *Cell* **163,** 123–133 (2015).
33. Lin, Y. *et al*. Formation and maturation of phase-separated liquid droplets by RNA-binding proteins article formation and maturation of phase-separated liquid droplets by RNA-binding proteins. *Mol. Cell* **60,** 1–12 (2015).
34. Gilbert, W. Origin of life: the RNA world. *Nature* **319,** 618 (1986).
35. Higgs, P. G. & Lehman, N. The RNA World: molecular cooperation at the origins of life. *Nat. Rev. Genet.* **16,** 7–17 (2015).
36. Fedor, M. J. & Williamson, J. R. The catalytic diversity of RNAs. *Nat. Rev. Mol. Cell Biol.* **6,** 399–412 (2005).
37. Unrau, P. J. & Bartel, D. P. RNA-catalysed nucleotide synthesis. *Nature* **395,** 260–263 (1998).

38. Hanczyc, M. M., Fujikawa, S. M. & Szostak, J. W. Experimental models of primitive cellular compartments: encapsulation, growth, and division. *Science* **302,** 618–622 (2003).
39. Hanczyc, M. M. & Szostak, J. W. Replicating vesicles as models of primitive cell growth and division. *Curr. Opin. Chem. Biol.* **8,** 660–664 (2004).
40. Macía, J. & Solé, R. V. Synthetic Turing protocells: vesicle self-reproduction through symmetry-breaking instabilities. *Phil. Trans. R. Soc. B* **362,** 1821–1829 (2007).
41. Murtas, G. Early self-reproduction, the emergence of division mechanisms in protocells. *Mol. Biosyst.* **9,** 195–204 (2013).
42. Browne, K. P., Walker, D. A., Bishop, K. J. M. & Grzybowski, B. A. Self-division of macroscopic droplets: partitioning of nanosized cargo into nanoscale micelles. *Angew. Chem. Int. Ed. Engl.* **49,** 6756–6759 (2010).
43. Patashinski, A. Z., Orlik, R., Paclawski, K., Ratner, M. A. & Grzybowski, B. A. The unstable and expanding interface between reacting liquids: theoretical interpretation of negative surface tension. *Soft Matter* **8,** 1601–1608 (2012).
44. Giomi, L. & DeSimone, A. Spontaneous division and motility in active nematic droplets. *Phys. Rev. Lett.* **112,** 147802 (2014).
45. Baross, J. & Hoffman, S. Submarine hydrothermal vents and associated gradient environments as sites for the origin and evolution of life. *Orig. Life Evol. Biosph.* **15,** 327–345 (1985).
46. Martin, W. F. Hydrogen, metals, bifurcating electrons, and proton gradients: the early evolution of biological energy conservation. *FEBS Lett.* **586,** 485–493 (2012).
47. Martin, W. F., Sousa, F. L. & Lane, N. Evolution. Energy at life's origin. *Science* **344,** 1092–1093 (2014).

Acknowledgements

We would like to thank D. Tang for a critical reading of our manuscript.

Author contributions

All authors developed the project and wrote the paper together. Numerical solutions of the continuum model were obtained by R.S. and D.Z.

Additional information

Supplementary information is available in the online version of the paper. Reprints and permissions information is available online at www.nature.com/reprints. Correspondence and requests for materials should be addressed to F.J.

Competing financial interests

The authors declare no competing financial interests.

Methods

Reaction rates and energy supply. The chemical reaction A $\rightleftharpoons$ B converts soluble precursors A to droplet material B with forward reaction flux $s_{\rightarrow}$ and reverse flux $s_{\leftarrow}$. The net reaction flux $s = s_{\rightarrow} - s_{\leftarrow}$ characterizes the concentration per unit time that is undergoing the reaction. Compatibility with thermodynamics requires[48]

$$\frac{s_{\rightarrow}}{s_{\leftarrow}} = \exp\left(-\frac{\Delta\mu}{k_B T}\right) \tag{3}$$

where $\Delta\mu$ is the chemical free energy change associated with the forward reaction. This condition leads to detailed balance of forward and backward reaction rates at chemical equilibrium. The net reaction flux s can therefore be written as

$$s = s_{\leftarrow}\left[\exp\left(-\frac{\Delta\mu}{k_B T}\right) - 1\right] \tag{4}$$

Chemical equilibrium is reached when $\Delta\mu = 0$ and the net reaction flux vanishes, $s = 0$. If as in (1) the reaction does not involve other reaction partners or external energy input, the chemical free energy change $\Delta\mu = \Delta\mu^{(1)}$ is given by the difference of the chemical potentials,

$$\Delta\mu^{(1)} = \mu_B - \mu_A \tag{5}$$

Such a reaction leads to spontaneous degradation of B and formation of A if $\mu_B > \mu_A$ and thus $\Delta\mu^{(1)} > 0$. The chemical potentials of a molecular species n can be written as $\mu_n = k_B T \ln(v_n c_n) + w_n$, where v_n is a molecular volume and c_n the concentration of species n. The first term is of entropic origin while the contribution w_n is mainly enthalpic and includes internal molecular free energies and interaction energies between molecules. Note that w_n generally depends on composition, and thus has different values inside and outside the droplet.

The net reaction rate corresponding to reaction pathway (1) can thus be written as

$$s^{(1)} = s^{(1)}_{\leftarrow}\left(\frac{c_A}{c_B}K^{(1)} - 1\right) \tag{6}$$

where $K^{(1)} = (v_A/v_B)\exp((w_A - w_B)/k_B T)$ is the equilibrium constant of reaction pathway (1). Note that in the case of phase separation, $K^{(1)}$ and $s^{(1)}_{\leftarrow}$ can have different values inside and outside the droplet. If only reaction pathway (1) occurs, droplets are passive despite the presence of the reaction and the system reaches a thermodynamic equilibrium. No droplet divisions occur. Such a system exhibits Ostwald ripening and after long times reaches an equilibrium that contains either a single large droplet or no droplet.

Active droplets require an external energy supply that maintains the droplets away from thermodynamic equilibrium at all times. The reaction A $\rightleftharpoons$ B can be coupled to an externally supplied fuel C with reaction product C′ with chemical potential difference $\Delta\mu_C = \mu_C - \mu_{C'} > 0$. This second reaction pathway (2) obeys equation (4) with $\Delta\mu = \Delta\mu^{(2)}$ and

$$\Delta\mu^{(2)} = \mu_B - \mu_A - \Delta\mu_C \tag{7}$$

The corresponding reaction flux can be written as

$$s^{(2)} = s^{(2)}_{\leftarrow}\left(\frac{c_A}{c_B}K^{(2)} - 1\right) \tag{8}$$

with equilibrium constant $K^{(2)} = K^{(1)}\exp(\Delta\mu_C/k_B T)$. If both pathways are active at the same time, the net reaction flux is $s = s^{(1)} + s^{(2)}$. In this paper we consider the case where an active droplet converts B to A inside the droplet mainly via the reaction pathway (1) while outside the droplet material A is used to generate B mainly via the reaction pathway (2) using the external fuel as an energy source (see Fig. 2 and Supplementary Information). No chemical equilibrium can be reached in this case because the equilibrium constants $K^{(1)}$ and $K^{(2)}$ imply incompatible equilibrium conditions. The droplet is thus active.

Dynamics of active droplets. We consider a fluid that contains the droplet-forming material B at concentration $c = c_B$. The system segregates into two coexisting phases that are separated by a sharp interface. We consider the limit of strong segregation of phases by a sharp interface. Across the interface, chemical potentials are continuous, $\mu_+ = \mu_-$, while the pressure exhibits a jump

$$P_- - P_+ = 2\gamma H \tag{9}$$

known as Laplace pressure. Here, γ denotes surface tension and H denotes the local mean curvature of the interface. The subscripts $-$ and $+$ refer to values at the interface inside and outside the droplet, respectively. These thermodynamic conditions determine the concentrations c_- and c_+ at the interface where both phases coexist. As the Laplace pressure depends on local curvature, the equilibrium concentrations also depend on curvature H. We express this dependence to linear order by

$$c_\pm \simeq c^{(0)}_\pm + \gamma\beta_\pm H \tag{10}$$

where $c^{(0)}_\pm$ denote the equilibrium concentrations of coexisting phases at a flat interface and we have introduced the coefficients $\beta_\pm$ to describe the effects of interface curvature.

The droplet material B is produced by chemical reactions with total reaction flux s, which is a function of concentration (see Fig. 3a and the section 'Reaction rates and energy supply'). The time evolution of the concentration field c is then described by the reaction–diffusion equation

$$\partial_t c = D_\pm \nabla^2 c + s \tag{11}$$

where D_+ and D_- denote the diffusion coefficients outside and inside the droplet, respectively. The evolution of the droplet shape is governed by the normal velocity of the droplet interface

$$v_n = \frac{j_- - j_+}{c_- - c_+} \tag{12}$$

where $j_\pm = -\mathbf{n}\cdot D_\pm \nabla c$ are the normal diffusion fluxes at the interface, inside and outside the droplet, and $\mathbf{n}$ denotes the surface normal.

The reaction flux is typically positive (B is produced) outside the droplet, while it is negative (A is produced) inside (see Fig. 3a). We expand the function $s(c)$ introduced in the section 'Reaction rates and energy supply' in terms of the concentration variations inside and outside the droplet to linear order as (see Supplementary Information)

$$s(c) \simeq \begin{cases} \nu_+ - k_+(c - c^{(0)}_+) & \text{outside the droplet} \\ -\nu_- - k_-(c - c^{(0)}_-) & \text{inside} \end{cases} \tag{13}$$

The reaction rates $k_\pm$ inside and outside the droplet are related to elasticity coefficients of the chemical reactions[49]. The fluxes of production of B molecules at the equilibrium concentrations outside and inside the droplet are denoted ν_+ and ν_-, respectively. We call ν_- turnover because it is the flux at which B molecules disappear inside the droplet. The concentration field varies over the characteristic length scales $l_\pm = (D_\pm/k_\pm)^{1/2}$ inside and outside the droplet, respectively.

At large distances $r \gg l_+$ from the droplet, the net reaction flux $s(c)$ vanishes and the concentration reaches the constant value $c_\infty = c^{(0)}_+ + \nu_+/k_+$. The chemical reactions thus generate a supersaturation

$$\epsilon = \frac{c_\infty - c^{(0)}_+}{\Delta c} \tag{14}$$

where $\Delta c = c^{(0)}_- - c^{(0)}_+$. This supersaturation drives the diffusion flux j_+ toward the droplet interface. Inside the droplet, droplet material is degraded, leading to a concentration profile with minimal concentration in the droplet centre. This causes a diffusion flux j_- towards the centre (see Fig. 3b).

Data availability. The data that support the plots within this paper and other findings of this study are available from the corresponding author on request.

References

48. Atkins, P. & de Paula, J. *Atkins' Physical Chemistry* (OUP Oxford, 2010).
49. Kacser, H., Burns, J. A. & Fell, D. A. The control of flux. *Biochem. Soc. Trans.* **23,** 341–366 (1995).

nature physics

SUPPLEMENTARY INFORMATION

DOI: 10.1038/NPHYS3984

In the format provided by the authors and unedited.

Growth and division of active droplets provides a model for protocells

David Zwicker,[1,2,*] Rabea Seyboldt,[1,*] Christoph A. Weber,[1] Anthony A. Hyman,[3] and Frank Jülicher[1,†]

[1]*Max Planck Institute for the Physics of Complex Systems, 01187 Dresden, Germany*

[2]*School of Engineering and Applied Sciences, Harvard University, Cambridge, MA 02138, USA*

[3]*Max Planck Institute of Molecular Cell Biology and Genetics, 01307 Dresden, Germany*

[*] These two authors contributed equally

[†] To whom correspondence should be addressed; Email: julicher@pks.mpg.de

CONTENTS

I. CONTINUUM MODEL FOR ACTIVE DROPLETS

A. Free energy function and chemical rates

We consider an incompressible fluid containing two components: a component A that forms the background fluid and a droplet material B that forms droplets by phase separation. Chemical reactions convert the two components into each other. The concentration of the droplet material B is denoted by $c(\boldsymbol{r},t)$ where $\boldsymbol{r}$ is the position and t denotes time. The concentration of the second component can be determined from c using the incompressibility condition. Therefore, the free energy density f only depends on the concentration c. We use the following double-well free energy function

$$f(c) = \frac{b}{2(\Delta c)^2}\left(c - c_-^{(0)}\right)^2\left(c - c_+^{(0)}\right)^2 , \tag{S.1}$$

where we have defined $\Delta c = \left|c_-^{(0)} - c_+^{(0)}\right|$. Here, the positive parameter b characterizes molecular interactions and entropic contributions. This free energy describes the segregation of the fluid in two coexisting phases[1]: one phase rich in droplet material with $c \approx c_-^{(0)}$ and a diluted phase with $c \approx c_+^{(0)}$.

The state of the system is characterized by the free energy

$$F[c] = \int \left[f(c) + \frac{\kappa}{2}\left(\boldsymbol{\nabla} c\right)^2\right] \mathrm{d}^3 r \, , \tag{S.2}$$

where the integral is over the system volume. Here, the coefficient κ is related to surface tension and the interface width[2]. The chemical potential $\bar{\mu} = \delta F[c]/\delta c$, which governs demixing, reads

$$\bar{\mu} = \frac{b}{(\Delta c)^2}\left(c - c_+^{(0)}\right)\left(c - c_-^{(0)}\right)\left(2c - c_-^{(0)} - c_+^{(0)}\right) - \kappa \boldsymbol{\nabla}^2 c \, . \tag{S.3}$$

The dynamics of the concentration field is described by the reaction-diffusion equation[3,4]

$$\partial_t c = m \boldsymbol{\nabla}^2 \bar{\mu} + s(c) \, . \tag{S.4}$$

Here, m is a mobility coefficient of the droplet material. The source term $s(c)$ describes chemical reactions.

We choose the function $s(c)$ to be linear in the phases outside and inside the droplet. We connect these linear behaviors by a cubic interpolating polynomial:

$$s(c) = \begin{cases} \nu_+ + k_+ c_+^{(0)} - k_+ c & \text{for } c < c_{\mathrm{c}}^+ \\ -\nu_- + k_- c_-^{(0)} - k_- c & \text{for } c > c_{\mathrm{c}}^- \\ p(c) & \text{for } c_{\mathrm{c}}^+ < c < c_{\mathrm{c}}^- \end{cases} , \tag{S.5}$$

where c_c^+ and c_c^- are two characteristic concentrations and $p(c) = a_0 + a_1 c + a_2 c^2 + a_3 c^3$ is a cubic polynomial. The coefficients a_i are determined uniquely by the conditions that $s(c)$ and its derivative are continuous functions:

$$p(c_c^+) = \nu_+ + k_+ c_+^{(0)} - k_+ c_c^+ \tag{S.6a}$$

$$p(c_c^-) = -\nu_- + k_- c_-^{(0)} - k_- c_c^- \tag{S.6b}$$

$$p'(c_c^+) = -k_+ \tag{S.6c}$$

$$p'(c_c^-) = -k_- \quad . \tag{S.6d}$$

The reaction flux given in Eq. (S.5) describes a situation where an external energy source drives the system away from equilibrium, see Methods section in the main text. Eqs. (S.3)–(S.5) define the continuum model of active droplets.

B. Relation with the effective droplet model

The model described by Eq. (S.4) typically forms distinct phases, which are separated by an interface. Considering a flat interface between two phases with bulk concentrations $c = c_-^{(0)}$ and $c = c_+^{(0)}$, the free energy F given in Eq. (S.2) is minimized by the concentration profile

$$c^*(x) = \frac{c_-^{(0)} + c_+^{(0)}}{2} + \frac{c_-^{(0)} - c_+^{(0)}}{2} \tanh \frac{x}{\hat{w}} \,, \tag{S.7}$$

where x is a coordinate that is normal to the interface and $\hat{w} = 2(\kappa/b)^{1/2}$ is the interface width[2]. The surface tension, i.e. the free energy per unit area of the interface, is[1]

$$\gamma = \int_{-\infty}^{\infty} F[c^*(x)] \mathrm{d}x = \frac{(\Delta c)^2}{6} \sqrt{\kappa b} \,. \tag{S.8}$$

Two different bulk concentrations c_- and c_+ coexist across the interface for which the chemical potential is equal on both sides. For a curved interface the pressure difference between the inside and outside of the droplet is the Laplace pressure $2\gamma H$, where H is the mean curvature of the interface. These two equilibrium conditions read

$$0 = \bar{\mu}(c_-) - \bar{\mu}(c_+) \tag{S.9a}$$

$$0 = (c_- - c_+)\bar{\mu}(c_-) + f(c_+) - f(c_-) - 2\gamma H \,, \tag{S.9b}$$

where c_- and c_+ denote the concentration at the interface inside and outside the droplet, respectively. Using the free energy density as defined in Eq. (S.1), the concentrations that obey Eqs. (S.9)

can be expressed to first order in H as

$$c_- \approx c_-^{(0)} + \beta\gamma H \tag{S.10a}$$

$$c_+ \approx c_+^{(0)} + \beta\gamma H \ , \tag{S.10b}$$

which is valid for small surface tension, $\gamma \ll \Delta c/(H\beta)$. Here, the coefficient $\beta = 2/(b\Delta c)$ describes the effect of Laplace pressure on the concentration at the interface. Note that $\gamma\beta$ defines a length scale, which is related to the interface width by $\gamma\beta = \hat{w}\Delta c/6$. Linearizing Eq. (S.4) at the values $c_+^{(0)}$ and $c_-^{(0)}$ outside and inside the droplet gives the linear reaction-diffusion equation defined in the Methods section in the main text, with diffusivity $D = mb$.

We thus can relate the parameters b, κ, and m of the continuum model to the parameters γ, $\beta_\pm$, and $D_\pm$ of the effective droplet model. In particular, $\beta_+ = \beta_- = \beta$, and $D_+ = D_- = D$. In Table S1 we list the parameters of both models.

C. Numerical methods

We solved Eq. (S.4) with (S.5) and (S.3) numerically using the xmds2 software package[5] (version 2.2.2) with an adaptive Runge-Kutta scheme of order 4/5, with tolerance 10^{-5}. The Laplace operator was evaluated by a spectral method, while the chemical rates were evaluated in real space. Numerical calculations were performed in a finite volume with no flux boundary conditions.

We normalize concentration, length and time by $\Delta c = c_-^{(0)} - c_+^{(0)}$, $\hat{w}$ and $t_0 = \hat{w}^2/D$, respectively, where the characteristic length scale is $\hat{w} = 2(\kappa/b)^{1/2}$. The relevant dimensionless model parameters are $c_+^{(0)}/\Delta c$, $k_\pm t_0$, $\nu_\pm t_0/\Delta c$ and $c_c^\pm/\Delta c$. In all numerical calculations, we chose $c_+^{(0)}/\Delta c = 0$ and $k_\pm t_0 = 10^{-2}$.

1. Stability diagram

Using three dimensional calculations in Cartesian coordinates, we observed that droplet configurations during the division of isolated single droplets were approximately axisymmetric. To determine the stability diagram shown in Fig. 2C we therefore performed calculations in cylindrical coordinates imposing axisymmetry. We used an axisymmetric cylindrical box with length $60\hat{w}$ and radius $30\hat{w}$, discretized with 120 and 60 points, respectively.

The initial conditions were given by a concentration profile that corresponded to a droplet geometry of a slightly prolate ellipsoid with unequal half axes of length $R/\hat{w} - 0.1$ and $R/\hat{w} + 0.1$,

Continuum model	Effective droplet model
$k_+ t_0$	$k_+ \tau_0$
$k_- t_0$	$k_- \tau_0$
$\nu_+ t_0/\Delta c$	$\nu_+ \tau_0/\Delta c$
$\nu_- t_0/\Delta c$	$\nu_- \tau_0/\Delta c$
$c_+^{(0)}/\Delta c$	$c_+^{(0)}/\Delta c$
$c_c^+/\Delta c$	
$c_c^-/\Delta c$	
	β_+/β_-
	D_-/D_+
$\Delta c = c_-^{(0)} - c_+^{(0)}$	$\Delta c = c_-^{(0)} - c_+^{(0)}$
$\hat{w} = 2(\kappa/b)^{1/2}$	$w = 6\beta_+\gamma/\Delta c$
$t_0 = \hat{w}^2/D$	$\tau_0 = w^2/D_+$

TABLE S1. Dimensionless parameters of the continuum model and the effective droplet model, together with the characteristic concentrations, lengths and times used for normalization (bottom 3 rows). Note that the parameters $c_c^\pm/\Delta c$ of the continuum model capture properties of chemical reactions inside the interface and therefore do not exist in the effective droplet model. In the continuum model we use a simple choice of the free energy (Eq. (S.1)) for which $\beta = \beta_+ = \beta_-$, with $\beta = 2/(b\Delta c)$, and $D = D_+ = D_-$, with $D = mb$. The dimensionless parameter $c_+^{(0)}/\Delta c$ is unimportant for the dynamical behavior of the system and only leads to a constant shift of the concentration profiles.

centered at the box center. The initial droplet size was chosen close to the stationary size in the continuum model. As an estimate for the stationary size we typically chose $R/\hat{w} = 0.9\bar{R}_\mathrm{s}/w$. Here, $\bar{R}_\mathrm{s}$ is the stationary radius calculated in the effective droplet model and $w = 6\beta_+\gamma/\Delta c$, see Section I B. The concentration field at positions $\boldsymbol{r}$ was initialized by the function

$$c(\boldsymbol{r}) = \frac{c_\infty + c_-^{(0)}}{2} + \frac{c_\infty - c_-^{(0)}}{2} \tanh \frac{d(\boldsymbol{r})}{\hat{w}} \,. \tag{S.11}$$

where $d(\boldsymbol{r})$ is the oriented distance of $\boldsymbol{r}$ to the nearest point on the ellipsoid. The value of $d(\boldsymbol{r})$ is negative for points inside the droplet and positive for points outside. The concentration far from the droplet is $c_\infty = \nu_+/k_+ + c_+^{(0)}$.

We calculated the dynamics of the concentration field over a time interval $T/t_0 = 10^4$, for different values of $\nu_\pm t_0/\Delta c$. The parameters $c_c^\pm$ related to the chemical reaction in Eq. (S.5) were chosen as $c_c^+/\Delta c = 0.25$ and $c_c^-/\Delta c = 0.75$. Because close to the shape instability the dynamics slows down, we may slightly overestimate the region of stability, since we cannot detect the exact instability with the finite time intervals simulated. Contours shown in Fig. 1C correspond to $c/\Delta c = 0.5$.

2. *Calculations for multiple divisions*

Several subsequent divisions break cylindrical symmetry. The calculations shown in Fig. 3A were therefore performed in three dimensions using cartesian coordinates. We chose a cubic box with side length $L = 50\hat{w}$ and an equidistant discretization of 100 points along each dimension.

Initial conditions corresponded to a spherical droplet centered at $\boldsymbol{r} = (L/4, L/4, L/4)$. The concentration field was initialized with $c = c_-^{(0)}$ inside the droplet and $c = c_\infty$ outside. The parameters for the calculations were $\nu_- t_0/\Delta c = 7 \cdot 10^{-3}$, $\nu_+ t_0/\Delta c = 2 \cdot 10^{-3}$ and $c_c^+/\Delta c = c_c^-/\Delta c = 0.5$. Surfaces shown in Fig. 3A correspond to $c/\Delta c = 0.5$.

II. EFFECTIVE MODEL FOR ACTIVE DROPLETS

Using the effective droplet model defined in the Methods section in the main text, we discuss steady state droplets and perform a linear stability analysis of the spherical droplet shape. We determine conditions for a shape instability towards an elongated shape.

A. Droplet dynamics in spherical coordinates

Using spherical coordinates r, θ, ϕ centered on the droplet, the interface defining the droplet surface is positioned at radial distance $r = R(\theta, \phi)$. Away from the interface, the concentration field $c(r, \theta, \phi)$ obeys the reaction-diffusion equation

$$\partial_t c = D_\pm \nabla^2 c + s \; . \tag{S.12}$$

Here, t denotes time and D_+, D_- are the diffusion coefficients outside ($r > R(\theta, \phi)$) and inside ($r < R(\theta, \phi)$) the droplet, respectively. The reaction flux s is given by

$$s = \begin{cases} \nu_+ - k_+(c_+ - c_+^{(0)}) & \text{for} \quad r > R \\ -\nu_- - k_-(c - c_-^{(0)}) & \text{for} \quad r < R \end{cases} . \tag{S.13}$$

Here, reaction rates inside and outside the droplet are denoted by $k_\pm$, $c_\pm^{(0)}$ denote the equilibrium bulk concentrations of coexisting phases near a planar interface. The reaction fluxes at equilibrium concentrations are denoted by $\nu_\pm$. For the concentration $c = c_0$, with $c_0 = -\nu_-/k_- + c_-^{(0)}$, the reaction flux inside the droplet vanishes, while for $c = c_\infty$ with $c_\infty = \nu_+/k_+ + c_+^{(0)}$ the reaction flux outside the droplet vanishes.

At the interface at $r = R(\theta, \phi)$ we impose boundary conditions for the concentration:

$$c(R_\pm) = c_\pm^{(0)} + \beta_\pm \gamma H(\theta, \phi) \; . \tag{S.14}$$

These boundary conditions describe a concentration jump at the interface. They corresponds to local thermodynamic equilibrium at a curved interface with surface tension γ. Here, $R_\pm$ denote the limits of approaching the interface at radial distance $R(\theta, \phi)$ from the outside or the inside, respectively. The mean curvature of the interface is denoted by H and the coefficients $\beta_\pm$ describe the change of the equilibrium concentration at the interface due to Laplace pressure $2\gamma H$.

The normal velocity v_n of the interface is proportional to the difference of normal fluxes inside and outside[6],

$$v_n = \boldsymbol{n} \cdot \frac{\boldsymbol{j}_- - \boldsymbol{j}_+}{c(R_-) - c(R_+)} \,, \tag{S.15}$$

with flux $\boldsymbol{j}_\pm = -D_\pm \boldsymbol{\nabla} c(R_\pm)$ and unit vector $\boldsymbol{n}$ normal to the interface. The droplet shape $\boldsymbol{R}(\theta,\phi) = R(\theta,\phi)\boldsymbol{e}_r$, where $\boldsymbol{e}_r$ denotes the unit vector in radial direction, can be parameterized using the angles θ and ϕ. The interface velocity can be written as

$$\frac{\partial \boldsymbol{R}(\theta,\phi,t)}{\partial t} = v_\theta \boldsymbol{e}_1 + v_\phi \boldsymbol{e}_2 + v_n \boldsymbol{n} \,, \tag{S.16}$$

where $\boldsymbol{e}_1 = \partial \boldsymbol{R}/\partial\theta$ and $\boldsymbol{e}_2 = \partial \boldsymbol{R}/\partial\phi$ are the two basis vectors of the tangential plane. Using $\partial \boldsymbol{R}/\partial t = (\partial R/\partial t)\boldsymbol{e}_r$, the velocity components v_θ and v_ϕ can be obtained from the conditions $(\partial \boldsymbol{R}/\partial t)\boldsymbol{e}_\theta = 0$ and $(\partial \boldsymbol{R}/\partial t)\boldsymbol{e}_\phi = 0$. Here, $\boldsymbol{e}_\theta$ and $\boldsymbol{e}_\phi$ are the local normalized basis vectors corresponding to θ and ϕ in spherical coordinates. The radial interface velocity $\partial R/\partial t = (\partial \boldsymbol{R}/\partial t)\cdot\boldsymbol{e}_r$ then reads

$$\frac{\partial R}{\partial t} = v_n \left[1 + \left(\frac{\partial_\theta R}{R} \right)^2 + \left(\frac{\partial_\phi R}{R \sin\theta} \right)^2 \right]^{\frac{1}{2}} \,, \tag{S.17}$$

where v_n is given by (S.15).

B. Stationary states of spherical droplets

Stationary solutions to Eq. (S.12) with spherically symmetric concentration field can be expressed as

$$\bar{c}(r) = A_\pm + B_\pm \frac{e^{r/l_\pm}}{r} + C_\pm \frac{e^{-r/l_\pm}}{r} \,, \tag{S.18}$$

where $l_\pm = (D_\pm/k_\pm)^{1/2}$ are characteristic length scales. Here, the coefficients $A_\pm$ are set by the chemical reactions,

$$A_\pm = \pm \frac{\nu_\pm}{k_\pm} + c_\pm^{(0)} \,. \tag{S.19}$$

Regular behavior at $r = 0$ implies $C_- = -B_-$. For an infinite system, the concentration far from the droplet reaches a constant value. This implies $B_+ = 0$. Using the boundary conditions (S.14) at the interface of a spherical droplet of radius R we obtain the remaining coefficients

$$C_+ = \left(\frac{\gamma\beta_+}{R} - \frac{\nu_+}{k_+} \right) R \exp(R/l_+) \tag{S.20a}$$

$$B_- = \left(\frac{\gamma\beta_-}{R} + \frac{\nu_-}{k_-} \right) \frac{R}{2\sinh(R/l_-)} \,. \tag{S.20b}$$

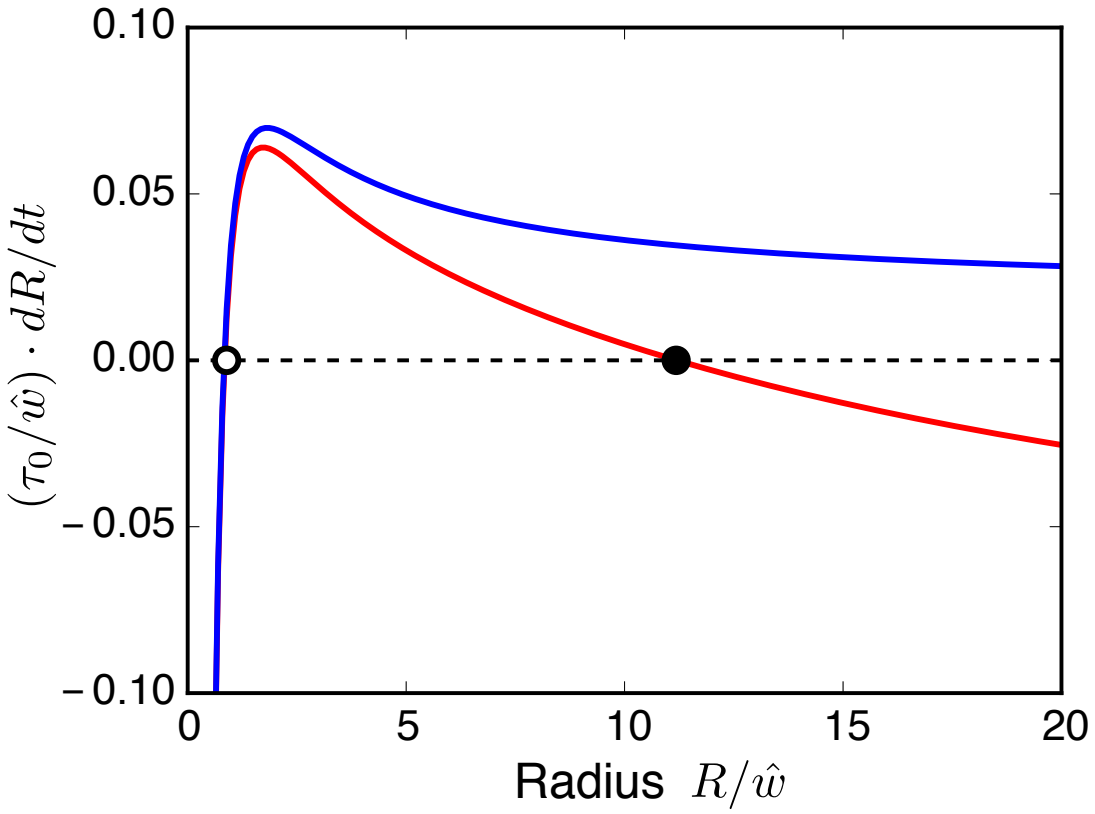

FIG. S1. Size dependence of droplet growth rates. Rate of droplet growth dR/dt as a function of droplet radius R in a quasistatic limit with turnover ν_- inside the droplet (red line) and without turnover ν_- inside the droplet (blue line). The zeros of dR/dt correspond to stationary radii. An unstable critical radius (white circle) and a stable droplet radius (black circle) are indicated. Parameter values are: $\nu_-\tau_0/\Delta c = -10^{-2}$ (red line) or $\nu_-\tau_0/\Delta c = 0$ (blue line), $\nu_+\tau_0/\Delta c = 2\cdot 10^{-3}$, $k_\pm\tau_0 = 0.01$, $c_+^{(0)} = 0$, $\beta_- = \beta_+$, $D_- = D_+$. Here, $w = 6\beta_+\gamma/\Delta c$ and $\tau_0 = D_+/w^2$ are characteristic length and time scales.

The normal fluxes at the droplet interface are

$$j_+(R) = \frac{D_+}{R}\left(\frac{\gamma\beta_+}{R} - \frac{\nu_+}{k_+}\right)\left(1 + \frac{R}{l_+}\right) \tag{S.21a}$$

$$j_-(R) = \frac{D_-}{R}\left(\frac{\gamma\beta_-}{R} + \frac{\nu_-}{k_-}\right)\left(1 - \frac{R}{l_-}\coth\frac{R}{l_-}\right) \ . \tag{S.21b}$$

Using these steady state fluxes in Eq. (S.17) and Eq. (S.15) provides a relation between $\mathrm{d}R/\mathrm{d}t = v_n$ and the droplet radius R in a quasi-static limit. Steady state droplets exist for radii $R = \bar{R}$ for which $\mathrm{d}R/\mathrm{d}t$ vanishes. These stationary radii thus obey

$$j_+(\bar{R}) = j_-(\bar{R}) \ . \tag{S.22}$$

Fig. S1 shows an example of $\mathrm{d}R/\mathrm{d}t$ as a function of R in the presence (red line) and absence (blue line) of chemical reactions inside the droplet. If chemical reactions are present, two steady state radii denoted $\bar{R}_\mathrm{c}$ (white circle) and $\bar{R}_\mathrm{s}$ (black circle) exist, corresponding to a critical nucleation radius and a stationary droplet radius, respectively. Both stationary radii are shown in Fig. 2A in the main text.

In the limit of large characteristic lengths $l_\pm$ compared to the droplet radius R, the stationary radii can be approximated as

$$\bar{R}_\mathrm{c} \approx \frac{\gamma\beta_+}{c_\infty - c_+^{(0)}} \,, \tag{S.23}$$

and

$$\bar{R}_\mathrm{s} \approx \sqrt{\frac{3D_+(c_\infty - c_+^{(0)})}{\nu_-}} \,, \tag{S.24}$$

where we have used $R \ll l_-$ and $\beta_\pm\gamma/[\bar{R}(c_-^{(0)} - c_+^{(0)})] \ll 1$. The latter is obeyed for a sharp interface, see section I B.

The critical radius estimated by Eq. (S.23) is closely related to the classical expression for the critical nucleation radius of passive droplets. The critical nucleation radius depends on the supersaturation $\epsilon = (c_\infty - c_+^{(0)})/\Delta c$, which, in the case of active droplets, is determined by chemical reactions instead of the amount of material provided.

The stationary droplet radius given in Eq. (S.24) describes an inherently non-equilibrium stationary state that is maintained by opposing fluxes[7].

C. Chemical turnover of stationary droplets

We define the droplet turnover time as the time after which the droplet material has been replaced on average. Consequently, the turnover time t_R is given by the total amount N of droplet material in the droplet, divided by the integrated flux J with which droplet material is turned into component A by the reaction $B \to A$,

$$t_\mathrm{R} = \frac{N}{J} \,. \tag{S.25}$$

Here, N is given by

$$N = \int_V c_-(\boldsymbol{r}) dV \,, \tag{S.26}$$

where $c_-(\boldsymbol{r})$ is the concentration field of droplet material inside the droplet, and V is the droplet volume. In the stationary state, the reaction flux J is equal to the integrated outflux of droplet

material across the droplet interface, which is given by

$$J = -\oint_S j_-(R) dA \,, \tag{S.27}$$

where $j_-(R)$ is the diffusion flux of droplet material normal to the droplet surface S.

In a stationary state, $j_-(R)$ is given by Eq. (S.21b) and $c_-(\boldsymbol{r})$ by Eq. (S.18). We then have

$$N = \frac{4}{3}\pi R^3 \left(c_-^{(0)} - \frac{\nu_-}{k_-}\right) + 4\pi R l_-^2 \left(\frac{\nu_-}{k_-} + \frac{\gamma\beta_-}{R}\right)\left(\frac{R}{l_-}\coth\frac{R}{l_-} - 1\right) \tag{S.28}$$

$$J = 4\pi R D_- \left(\frac{\gamma\beta_-}{R} + \frac{\nu_-}{k_-}\right)\left(\frac{R}{l_-}\coth\frac{R}{l_-} - 1\right) \,. \tag{S.29}$$

Therefore, the turnover time of a stationary droplet is given by

$$t_\mathrm{R} = \frac{c_-^{(0)} - \frac{\nu_-}{k_-}}{\nu_- + k_- \frac{\gamma\beta_-}{R}} \cdot \frac{\frac{1}{3}\left(\frac{R}{l_-}\right)^2}{\frac{R}{l_-}\coth\frac{R}{l_-} - 1} + \frac{1}{k_-} \,. \tag{S.30}$$

In the limit of $R \ll l_-$ and $\gamma\beta_-/(c_-^{(0)} - c_+^{(0)}) \ll R$, we find

$$t_\mathrm{R} \approx \frac{c_-^{(0)}}{\nu_-} \,. \tag{S.31}$$

D. Stability analysis of the spherical droplet shape

To analyze the linear stability of the stationary droplets, we linearize the dynamic equations in the vicinity of the stationary state and identify the dynamic eigenmodes. The stationary state is unstable with respect to a dynamic mode if the corresponding growth rate is positive.

1. Linearization at the stationary solution

We linearize the dynamic equations (S.12)–(S.15) and (S.17) around a stationary solution $\bar{c}(r)$, which obeys Eqs. (S.18)–(S.22). Introducing small perturbations δc and δR of the concentration field and the droplet shape, respectively, we write

$$c(r,\theta,\varphi,t) = \bar{c}(r) + \delta c(r,\theta,\varphi,t) \,, \tag{S.32}$$

and

$$R(\theta,\varphi,t) = \bar{R} + \delta R(\theta,\varphi,t) \,. \tag{S.33}$$

The concentration perturbation then obeys

$$\partial_t \delta c = D_\pm \nabla^2 \delta c - k_\pm \delta c \,. \tag{S.34}$$

The boundary conditions (S.14) become

$$\delta c(\bar{R}_\pm) = \beta_\pm \gamma \delta H - \bar{c}'(\bar{R}_\pm)\delta R \,, \tag{S.35}$$

where $\delta H = H(\bar{R} + \delta R) - H(\bar{R})$. Using Eqs. (S.15) and (S.17), the time dependence of the droplet shape perturbation is described to linear order by

$$(c_-^{(0)} - c_+^{(0)})\partial_t \delta R = D_+ \partial_r \delta c(\bar{R}_+) - D_- \partial_r \delta c(\bar{R}_-) + \left[D_+ \bar{c}''(\bar{R}_+) - D_- \bar{c}''(\bar{R}_-)\right] \delta R \,. \tag{S.36}$$

2. *Dynamic modes and relaxation spectrum*

The linearized dynamics of droplet perturbations near the steady state defines a linear operator $\mathscr{L}$ by

$$\partial_t \begin{pmatrix} \delta c \\ \delta R \end{pmatrix} = \mathscr{L} \begin{pmatrix} \delta c \\ \delta R \end{pmatrix} \,. \tag{S.37}$$

The operator $\mathscr{L}$ has eigenfunctions $(c_i, R_i)^\intercal$ with corresponding eigenvalues μ_i, where i is the mode index. These modes obey

$$\mathscr{L} \begin{pmatrix} c_i \\ R_i \end{pmatrix} = \mu_i \begin{pmatrix} c_i \\ R_i \end{pmatrix} \,. \tag{S.38}$$

The linear droplet dynamics can thus be decomposed in eigenmodes with amplitude A_i as

$$\begin{pmatrix} \delta c \\ \delta R \end{pmatrix} = \sum_i A_i \begin{pmatrix} c_i \\ R_i \end{pmatrix} e^{\mu_i t} \,, \tag{S.39}$$

where the sum is over all eigenmodes. Thus, the eigenfunctions of $\mathscr{L}$ correspond to dynamic modes of the system. For $\mu_i < 0$, the values $-\mu_i$ are relaxation rates. The steady state is stable if all $\mu_i < 0$.

3. *Determination of eigenmodes*

We determine the eigenmodes and the spectrum of relaxation rates of a stationary droplet with radius $\bar{R}$. Because of the spherically symmetric reference state, we introduce radial and angular indices $i = (n, m, l)$ and use the ansatz

$$\begin{pmatrix} c_{nlm}(r, \theta, \phi) \\ R_{nlm}(\theta, \phi) \end{pmatrix} = \begin{pmatrix} c_{nl}(r) \\ \epsilon_{nl} \end{pmatrix} Y_{lm}(\theta, \phi) \,, \tag{S.40}$$

where Y_{lm} are spherical harmonics and the corresponding eigenvalues will be denoted μ_{nl}. Using Eq. (S.34) with $r^2\nabla^2 Y_{lm} = l(l+1)Y_{lm}$, the radial part of the eigenfunctions obeys

$$\left(\frac{1}{r^2}\frac{\partial}{\partial r}r^2\frac{\partial}{\partial r} - (\lambda_{nl}^{\pm})^2 - \frac{l(l+1)}{r^2}\right) c_{nl}(r) = 0 \,, \tag{S.41}$$

where

$$(\lambda_{nl}^{\pm})^2 = \frac{k_{\pm} + \mu_{nl}}{D_{\pm}} \,. \tag{S.42}$$

The boundary conditions (S.35) at $r = \bar{R}$ can be written as

$$c_{nl}(\bar{R}_+) = a_l^+ \epsilon_{nl} \tag{S.43a}$$

$$c_{nl}(\bar{R}_-) = a_l^- \epsilon_{nl} \tag{S.43b}$$

with

$$a_l^{\pm} = \gamma\beta_{\pm}\frac{h_l}{\bar{R}^2} - \bar{c}'(\bar{R}_{\pm}) \,, \tag{S.44}$$

where[8] $h_l = (l^2 + l - 2)/2$. From Eqs. (S.43) we obtain a boundary condition at $r = \bar{R}$:

$$\frac{c_{nl}(\bar{R}_+)}{c_{nl}(\bar{R}_-)} = \frac{a_l^+}{a_l^-} \,. \tag{S.45}$$

Using Eq. (S.36), we obtain a second boundary condition

$$\left(c_-^{(0)} - c_+^{(0)}\right)\mu_{nl} = D_+\bar{c}''(\bar{R}_+) - D_-\bar{c}''(\bar{R}_-) + D_+a_l^+\frac{c'_{nl}(\bar{R}_+)}{c_{nl}(\bar{R}_+)} - D_-a_l^-\frac{c'_{nl}(\bar{R}_-)}{c_{nl}(\bar{R}_-)} \,. \tag{S.46}$$

The boundary conditions (S.45) and (S.46) provide jump conditions for both the values and the first derivatives of the radial modes $c_{nl}(r)$ at $r = \bar{R}$.

4. *Radial profiles and relaxation rates of dynamic modes*

When solving Eq. (S.41) with Eq. (S.42) to determine the dynamic modes of the system, we have to distinguish the cases $\mu_{nl} < -k_{\pm}$ and $\mu_{nl} > -k_{\pm}$, for which the sign of $(\lambda_{nl}^{\pm})^2$ differs. Near an instability of the droplet shape, an eigenmode exists for which μ_{nl} changes sign. Therefore, to discuss this instability, it is sufficient to consider the case $\mu_{nl} > -k_{\pm}$. In this case, $(\lambda_{nl}^{\pm})^2$ is positive and solutions to Eq. (S.41) are given by modified spherical Bessel functions $k_l(\lambda_{nl}^{\pm}r)$ and $i_l(\lambda_{nl}^{\pm}r)$. In order to obtain solutions that are finite at $r = 0$ and which do not diverge for large r, we have

$$c_{nl}(r) = \begin{cases} k_l(\lambda_{nl}^+ r) & \text{for} \quad r > \bar{R} \\ C_{nl}\, i_l(\lambda_{nl}^- r) & \text{for} \quad r < \bar{R} \end{cases} \,, \tag{S.47}$$

where the coefficient C_{nl} is determined by boundary conditions (S.45) as

$$C_{nl} = \frac{a_l^- k_l(\lambda_{nl}^+ \bar{R})}{a_l^+ i_l(\lambda_{nl}^- \bar{R})} \,. \tag{S.48}$$

The boundary condition (S.46) becomes

$$\left(c_-^{(0)} - c_+^{(0)}\right) \mu_{nl} = D_+ \bar{c}''(\bar{R}_+) - D_- \bar{c}''(\bar{R}_-) + D_+ a_l^+ \lambda_{nl}^+ \frac{k_l'(\lambda_{nl}^+ \bar{R})}{k_l(\lambda_{nl}^+ \bar{R})} - D_- a_l^- \lambda_{nl}^- \frac{i_l'(\lambda_{nl}^- \bar{R})}{i_l(\lambda_{nl}^- \bar{R})} \,. \tag{S.49}$$

Using $\lambda_{nl}^\pm = ((k_\pm + \mu_{nl})/D_\pm)^{1/2}$, Eq. (S.49) becomes an implicit equation for the unknown eigenvalues μ_{nl}. This equation typically has either no solution or one solution. We identify the largest eigenvalue for given l with $n = 1$.

In order to determine the full spectrum μ_{nl} of eigenmodes, we have to consider the case $\mu_{nl} < -k_\pm$. We then define $(\lambda_{nl}^\pm)^2 = -(k_\pm + \mu_{nl})/D_\pm$ and the solutions to Eq. (S.41) are of the form $C_{nl}^\pm j_l(\lambda_{nl}^\pm r) + D_{nl}^\pm y_l(\lambda_{nl}^\pm r)$, where $j_l(z)$ and $y_l(z)$ denote spherical Bessel functions, and the coefficients C_{nl} and D_{nl} are determined by boundary conditions. The functions $j_l(z)$ and $y_l(z)$ behave for large r as $j_l(z) \sim z^{-1}\sin(z - l\pi/2)$ and $y_l(z) \sim z^{-1}\cos(z - l\pi/2)$. Eq. (S.46) now has an infinite set of solutions μ_{nl} for $n > 1$, which we order such that $\mu_{nl} > \mu_{n+1,l}$. In an infinite system, the set μ_{nl} approaches a continuous spectrum.

5. *Instability of stationary spherical droplets*

The droplet shape is unstable if at least one mode with $\mu_{1l} > 0$ exists. We can obtain a criterion for this instability by using $\mu_{nl} = 0$ in Eq. (S.49). This leads to

$$0 = D_+ \bar{c}''(\bar{R}_+) - D_- \bar{c}''(\bar{R}_-) + \frac{D_+ a_l^+}{l_+} \frac{k_l'(\bar{R}/l_+)}{k_l(\bar{R}/l_+)} - \frac{D_- a_l^-}{l_-} \frac{i_l'(\bar{R}/l_-)}{i_l(\bar{R}/l_-)} \,, \tag{S.50}$$

which is a condition for the radius $\bar{R}$ at which the shape becomes unstable with respect to a deformation characterized by l.

Different modes l can become unstable. The case $l = 0$ corresponds to changes of the radius. A droplet with $\mu_{10} < 0$ has a stable radius $\bar{R}$. For $l = 1$ there always exists one marginal mode with $\mu_{1m} = 0$, which corresponds to a translation of the steady state and does not lead to an instability. The first mode that becomes unstable and changes the droplet shape is the elongation mode $l = 2$.

Fig. S2 shows numerically determined values of the largest relaxation rate μ_{1l} for $l = 0, 1, 2$ and 3 as a function of supersaturation ϵ far from the droplet. The figure reveals that μ_{12} changes sign and becomes positive as ϵ is increased, indicating the shape instability.

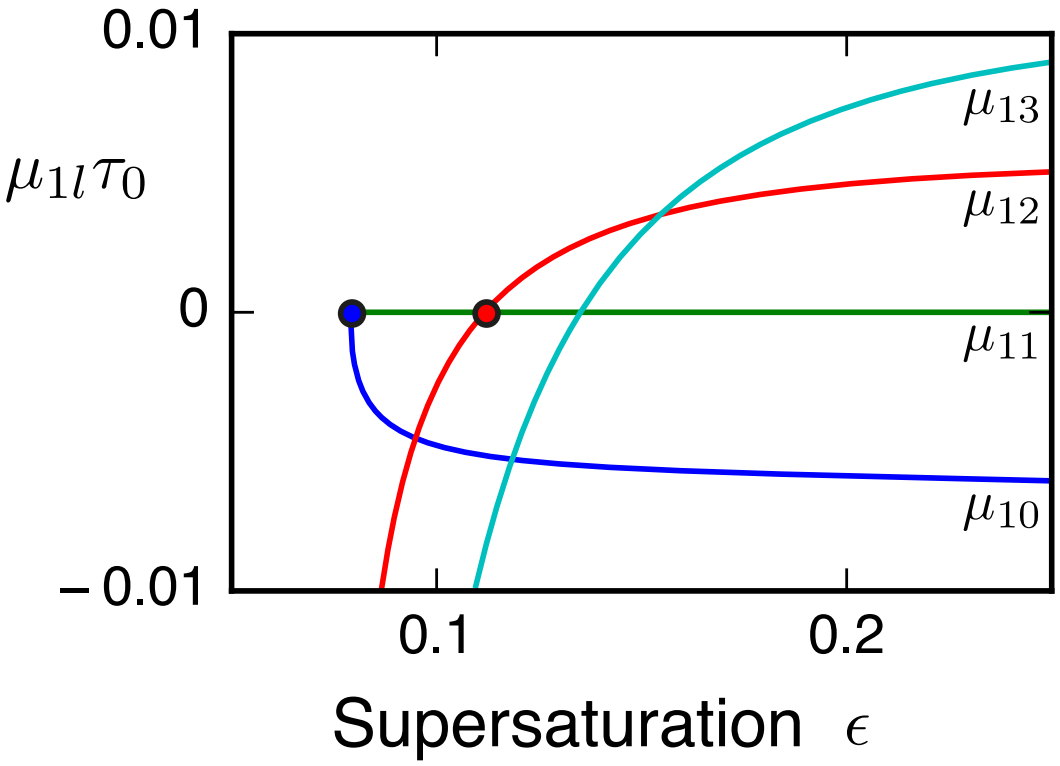

FIG. S2. Eigenvalues μ_{1l} as a function of supersaturation ϵ. At the onset of the instability (red dot) the second mode becomes unstable, leading to droplet deformation. For larger values of ϵ, higher modes become unstable as well. The same parameters as in Fig. 2A (main text), with $\nu_-/\nu_0 = 1$. Stationary and stable radii were used ($\mu_{10} < 0$).

Eq. (S.49) can be solved numerically. An approximation of the eigenvalues that is valid in the limit of weak chemical reactions $R \ll l_+$ is

$$\mu_{1l} \simeq (l-1)\frac{D_+}{\Delta c \bar{R}^2}\left[\left(c_\infty - c_+^{(0)}\right) - \frac{\gamma}{2\bar{R}}\left((4+3l+l^2)\beta_+ + l(l+2)\frac{\beta_- D_-}{D_+}\right)\right] . \qquad \text{(S.51)}$$

For modes $l \geq 2$, the spherical droplet becomes unstable for $\bar{R} > R_l$ which in this limit is given by

$$R_l \approx \gamma \frac{(4+3l+l^2)D_+\beta_+ + l(l+2)D_-\beta_-}{2D_+(c_\infty - c_+^{(0)})} . \qquad \text{(S.52)}$$

This expression shows that the elongation mode $l = 2$ is the first mode to become unstable. This provides an approximation for the critical radius $R_{\rm div}$ of droplet division,

$$R_{\rm div} \simeq \gamma \frac{7\beta_+ + 4\beta_- \frac{D_-}{D_+}}{c_\infty - c_+^{(0)}} . \qquad \text{(S.53)}$$

in the limit $R \ll l_+$. Using expression (S.24) for the stationary radius $\bar{R}_\mathrm{s}$, we can approximate the critical value of the supersaturation

$$\epsilon_\mathrm{div} \simeq \frac{1}{D_+}\left(\frac{\nu_-}{3}\right)^{1/3}\left((7\beta_+ D_+ + 4\beta_- D_-)\gamma\right)^{2/3} \tag{S.54}$$

for which stationary droplets undergo a shape instability. This expression approximates the instability line shown in Fig. 2B (red line). Eq. (S.54) implies a scaling $\nu_- \sim \epsilon_\mathrm{div}^3$ for $R \ll l_+$. Finally, the droplet radius for which the stationary droplet becomes unstable can be approximated for $R \ll l_+$ as

$$R_\mathrm{div} \simeq \left(\frac{3(7\beta_+ D_+ + 4\beta_- D_-)\gamma}{\nu_-}\right)^{1/3} . \tag{S.55}$$

This relation can be used to estimate typical sizes of droplets that undergo a shape instability and divide. Note that the approximation for the droplet radius at the onset of the shape instability in the limit $R \ll l_+$ given in Eq. (S.53) approaches the instability condition of growing aggregates discussed by Mullins-Sekerka[9]. Note, however, that the approximate expression Eq. (S.55) in this limit for the onset of instability does not exist in the Mullins-Sekerka case. We discuss the relationship between our model and the Mullins-Sekerka instability in the next section.

III. RELATIONSHIP TO MULLINS-SEKERKA INSTABILITY

The shape instability leading to droplet division described in this work is related to the Mullins-Sekerka shape instability of growing aggregates. Here we discuss the initial shape change in the linear regime valid close to the shape instability for small amplitudes. We compare the behavior of this linear instability for active droplets and the Mullins-Sekerka case.

Consider a spherical particle or droplet perturbed by a small shape deformation. Using a decomposition of infinitesimal shape changes by spherical harmonics, the mode with $l = 0$ corresponds to a changing radius $R_0(t)$, the modes with $l = 1$ generate pure translations, and the modes with $l = 2$ are the shape deformation modes that become unstable first according to Eq. (S.52). We can thus ignore the modes with $l = 1$ and focus here on the radius change and the dynamics of the modes with $l = 2$, which are most relevant for the droplet division problem. Without loss of generality, we consider the case $m = 0$. Following the arguments of Mullins and Sekerka[9], we express the shape of a droplet as a function of the azimuthal and polar angles for a small deformation by a mode with $l = 2$:

$$R(\theta, \phi; t) \simeq R_0(t) + \epsilon_2(t)\hat{Y}_{20}(\theta, \phi) \, , \tag{S.56}$$

where $\epsilon_2 \ll R_0$, $\hat{Y}_{20}(\theta, \phi) = Y_{20}(\theta, \phi)/Y_{20}(0, 0)$ and we have neglected modes with $l > 2$. For such a perturbation, the interface moves locally with a radial velocity $v = \partial R/\partial t$, which reads

$$v(\theta, \phi) \simeq \frac{\mathrm{d}R_0}{\mathrm{d}t} + \frac{\mathrm{d}\epsilon_2}{\mathrm{d}t}\hat{Y}_{20}(\theta, \phi) \, . \tag{S.57}$$

A. Droplet with chemical reaction

In our model of chemically active droplets, we consider a droplet in the vicinity of the stationary radius $\bar{R}_\mathrm{s}$. We can express the droplet radius as $R_0(t) = \bar{R}_\mathrm{s} + \epsilon_0(t)$. For small perturbations of the stationary state, $\epsilon_0, \epsilon_2 \ll \bar{R}_\mathrm{s}$, the growth rates are given by $\mathrm{d}R_0/\mathrm{d}t = \mu_{10}\epsilon_0(t)$ and $\mathrm{d}\epsilon_2/\mathrm{d}t = \mu_{12}\epsilon_2(t)$, see Eq. (S.39) in Section II. At the stationary radius $R_0 = \bar{R}_\mathrm{s}$, the volume growth is zero, $\mathrm{d}R_0/\mathrm{d}t = 0$, so that the $l = 2$ mode determines the radial velocity,

$$v(\theta, \phi) \simeq \mu_{12}\epsilon_2(t)\hat{Y}_{20}(\theta, \phi) \, . \tag{S.58}$$

If the mode $l = 2$ is unstable, $\mu_{12} > 0$, we find for $\epsilon_2 > 0$ that $v(0, \phi) > 0$ and $v(\pi/2, \phi) < 0$. The droplet thus elongates along the long axis, and constricts along the waistline, see Fig. S3A. If

we start sufficiently close to the stationary radius, $R_0 \approx \bar{R}_s$, contributions from the dynamics of $R_0(t)$ can be neglected as $\mu_{10} < 0$ and $R_0(t)$ thus approaches the stationary value.

B. Mullins-Sekerka model

In the case of the Mullins-Sekerka model, droplets grow with $\mathrm{d}R_0/\mathrm{d}t > 0$ if $R_0 > R_\mathrm{c}$, where R_c denotes the critical nucleation radius. These growing droplets may undergo a shape instability corresponding to mode l when the radius reaches the value[9]

$$R_l^\mathrm{ms} = \gamma \frac{(4+3l+l^2)D_+\beta_+ + l(l+2)D_-\beta_-}{2D_+(c_\infty - c_+^{(0)})} \,. \tag{S.59}$$

When modes with $l > 2$ become unstable they lead to shape deformations that grow into dendritic structures[10], while the modes with $l = 2$ are insufficient to generate complex shape changes[9]. To show this, we follow the arguments outlined in Ref. [9] and consider an instability of a mode with $l = 2$, which grows with the rate

$$\mu_{12} = \frac{1}{R_0} \frac{R_0 - R_2^\mathrm{ms}}{R_0 - R_\mathrm{c}} \frac{\mathrm{d}R_0}{\mathrm{d}t} \,. \tag{S.60}$$

Here, R_2^ms with $R_2^\mathrm{ms} > R_\mathrm{c}$ is the radius for which the $l = 2$ mode becomes unstable in the Mullins-Sekerka model, see Eq. (S.59). The interfacial velocity behaves in the Mullins-Sekerka model as

$$v(\theta,\phi) \simeq \left(1 + \frac{R_0 - R^\mathrm{ms}}{R_0 - R_\mathrm{c}} \frac{\epsilon_2}{R_0} \hat{Y}_{20}(\theta,\phi)\right) \frac{\mathrm{d}R_0}{\mathrm{d}t} \,. \tag{S.61}$$

Thus, for sufficiently small amplitudes ϵ_2 of the $l = 2$ mode, the droplet radius R increases in all spatial directions, $v(\theta,\phi) > 0$ for all angles θ, ϕ. This corresponds to a weak ellipsoidal deformation of the growing spherical droplet. As the droplet grows, the aspect ratio of this ellipsoid stays constant or approaches 1 as was shown in Ref. [9], see also Fig. S3B. Therefore, an unstable $l = 2$ mode does not trigger a shape instability of an initially spherical object in the Mullins-Sekerka model. Thus, instabilities of modes with $l > 2$ are required for the Mullins-Sekerka instability to take effect.

C. Comparison of both instabilities

These arguments show that there are interesting differences between the instability in our model and in the Mullins-Sekerka model. In the Mullins-Sekerka model an instability of a mode with

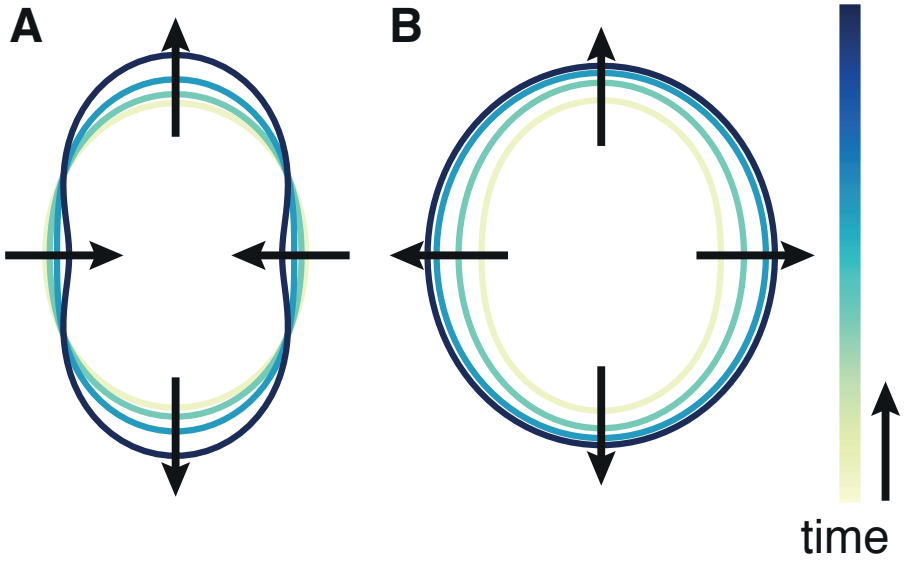

FIG. S3. Shape deformations resulting from an instability of the deformation mode with $l = 2$ for a chemically active droplet (A) and a growing droplet in the Mullins-Sekerka model (B). The black arrows indicate the direction of interfacial motion. (A) In the model of chemically active droplets, a stationary droplet constricts around the waistline as the amplitude of the perturbation increases. (B) In the Mullins-Sekerka model, an unstable $l = 2$ mode gives rise to an ellipsoidal shape with an aspect ratio that approaches 1 as the droplet grows. This implies that the shape is not unstable with respect to the $l = 2$ mode even if this mode is linearly unstable[9]. The shape deformations shown in A and B correspond to the linear regime valid if amplitudes are small. Radial growth in B is reduced to emphasize the shape changes.

$l = 2$ does not directly trigger a shape instability because the droplet grows at the same time as the instability develops. Conversely, for the chemically active droplets discussed in the present manuscript, the instability of the modes with $l = 2$ generates to linear order a shape change that leads to a dumbbell shape. In the nonlinear regime beyond the instability, the shape then undergoes a dramatic shape change which subsequently pinches off in two droplets.

Another difference between the models is that in our system the chemical reaction rates together with the diffusion coefficients introduce the length scales $l_{\pm}$, which do not exist in the Mullins-Sekerka case. Consequently, the instability condition of droplet shape, obtained by solving Eq. (S.49), is generally different from the Mullins-Sekerka case. The expression for the instability condition for chemically active droplets approaches the one of the Mullins-Sekerka model given in Eq. (S.59) in the limit of large $l_{\pm}$, see Eq. (S.52).

The different waistline dynamics between our model and in the Mullins-Sekerka model also leads to different behaviors in the nonlinear regime. In the case of the Mullins-Sekerka model, modes with smaller wavelengths become unstable as the volume increases. In the nonlinear regime, this leads to large dendritic structures. In our model the droplet does not grow and modes with shorter wavelength thus remain stable. The chemically active droplet constricts at the waistline, which subsequently leads to droplet division.

IV. EXAMPLES OF PARAMETER VALUES FOR DIVIDING DROPLETS

In Table S2, we provide five examples of parameter values for which droplets become unstable. The corresponding stationary radii are shown in Fig. S4 as a function of the supersaturation. Case I is based on the properties of colloidal droplets or liquid protein phases with low interfacial tension[11–13]. We find that droplet division at sizes of several micrometers could be realized experimentally, see Fig. S4 and Table S1. In case I the division radius is $R_{\rm div} \approx 3\,\mu{\rm m}$. Case II is based on the properties of water/oil interfaces[13–16]. This example shows that even for these larger interfacial tensions as compared to case I, droplets can still have a division radius of the order of micrometers. Case III shows the effect of different diffusion constants and length-scales inside and outside the droplet, with division radii again in the micrometer range. Cases IV and V explore parameter regimes for which dividing droplets are larger. Case IV is based on case I, but with a longer turnover time. This leads to an increased division radius of $10\,\mu{\rm m}$. Case V is an example for division at even larger radii with $R_{\rm div} \approx 140\,\mu{\rm m}$. To obtain this droplet size, large diffusion constants D are required, and the interfacial width w and the turnover time $t_{\rm R}$ also have to be large. This can be understood by considering Eq. (S.53), which implies that for $R \ll l_{\pm}$, the division radius scales as $R_{\rm div} \sim (Dwt_{\rm R})^{1/3}$.

Our analysis thus shows that dividing droplets with sizes of several micrometers could be achieved experimentally. Simple choices of realistic parameter values typically lead to such droplet sizes. However, larger droplets from 100 micrometers to millimeters may turn out to be more difficult to achieve. To obtain such droplets in case V we had to choose large diffusion coefficients and slow reaction rates. We therefore propose that dividing active droplets as presented in this work provide simple models of micrometer sized protocells.

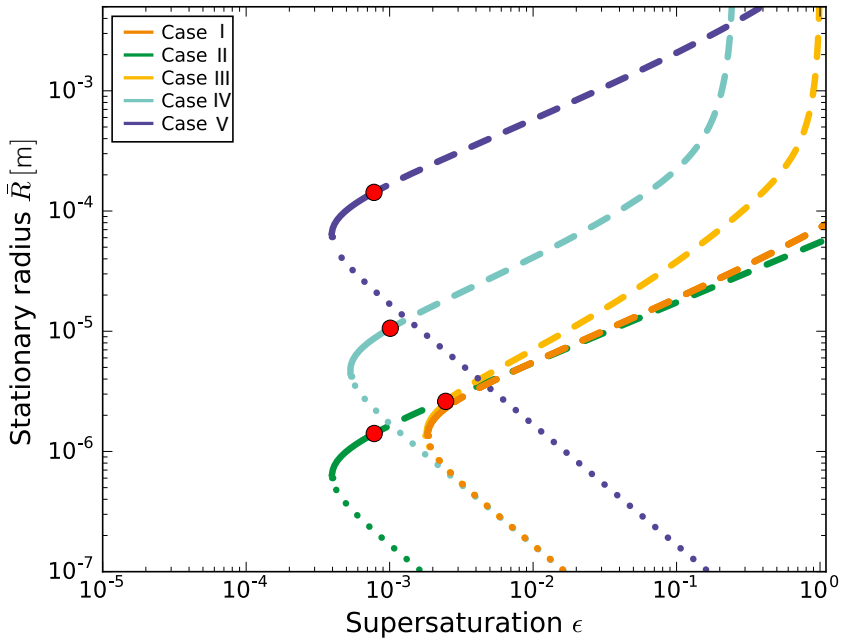

FIG. S4. Stationary radius $\bar{R}$ as a function of the supersaturation ϵ. The curves correspond to the five parameter sets given in Table S2, and are calculated using Eq. (S.22). Dotted lines indicate an unstable droplet size ($l = 0$ mode) and dashed lines indicate a shape instability ($l = 2$ mode), see Eq. (S.49). Stable droplets are shown as solid lines. The red dots show the onset of the shape instability. We report the respective stationary radii and supersaturations in Table S2.

Quantity	Unit	Case I	Case II	Case III	Case IV	Case V
D_-	$\mu m^2/s$	10	10	1	10	1000
D_+	$\mu m^2/s$	10	10	100	10	1000
w	nm	10	1	10	10	100
γ	mN/m	10^{-3}	10	10^{-3}	10^{-3}	10
$\beta_- = \frac{w\Delta c}{6\gamma}$	$M{\cdot}m^2/N$	$2\cdot10^{-4}$	$2\cdot10^{-8}$	$2\cdot10^{-4}$	$2\cdot10^{-4}$	$1.7\cdot10^{-6}$
$\beta_+ = \frac{w\Delta c}{6\gamma}$	$M{\cdot}m^2/N$	$2\cdot10^{-4}$	$2\cdot10^{-8}$	$2\cdot10^{-4}$	$2\cdot10^{-4}$	$1.7\cdot10^{-6}$
$c_-^{(0)}$	mM	100	10^3	100	100	10^3
$c_+^{(0)}$	mM	1	10^{-3}	1	1	10^{-3}
t_R	s	100	100	10	4000	10^4 (≈ 3 h)
l_-	mm	0.1	5	0.1	0.1	5
l_+	mm	0.1	5	0.01	0.1	5
$\nu_- = \frac{c_-^{(0)}}{t_R}$	mM/s	1	10	10	$2.5\cdot10^{-2}$	0.1
$\nu_+ = \epsilon\Delta c k_+$	nM/s	200	0.3	$2\cdot10^5$	100	30
$k_- = \frac{D_-}{l_-^2}$	$1/s$	10^{-3}	$4\cdot10^{-7}$	10^{-4}	10^{-3}	$4\cdot10^{-5}$
$k_+ = \frac{D_+}{l_+^2}$	$1/s$	10^{-3}	$4\cdot10^{-7}$	1	10^{-3}	$4\cdot10^{-5}$
$\bar{R}_s$ using Eq. (S.22)	μm	3	1	3	10	140
$\bar{R}_c$ using Eq. (S.22)	μm	0.7	0.2	0.7	1.7	20
$R_{div} = \bar{R}_s$	μm	3	1	3	10	140
ϵ_{div}		$2\cdot10^{-3}$	$8\cdot10^{-4}$	$2\cdot10^{-3}$	10^{-3}	$8\cdot10^{-4}$
$k_+\tau_0$		10^{-8}	$4\cdot10^{-13}$	10^{-5}	10^{-8}	$5\cdot10^{-10}$
$k_-\tau_0$		10^{-8}	$4\cdot10^{-13}$	10^{-9}	10^{-8}	$5\cdot10^{-10}$
$\nu_+\tau_0/\Delta c$		$2\cdot10^{-11}$	$3\cdot10^{-17}$	$2\cdot10^{-9}$	10^{-11}	$3\cdot10^{-13}$
$\nu_-\tau_0/\Delta c$		10^{-7}	10^{-9}	10^{-7}	$2.5\cdot10^{-9}$	10^{-9}
$c_+^{(0)}/\Delta c$		0.01	10^{-6}	0.01	0.01	10^{-6}
β_+/β_-		1	1	1	1	1
D_-/D_+		1	1	0.01	1	1
$\Delta c = c_-^{(0)} - c_+^{(0)}$	mM	99	10^3	99	99	10^3
w	nm	10	1	10	10	100
$\tau_0 = w^2/D_+$	μs	10	0.1	1	10	10

TABLE S2. Examples for parameter values of the effective model for five different cases. Both dimensional and dimensionless parameters are shown. Our choice of parameters that are related to phase separation ($D_\pm$, w, γ, and $c_\pm^{(0)}$) is based on measured values in liquid protein phases[11–13] (cases I, III and IV) and in water/oil interfaces[13–16] (case II). Case V explores extreme parameter ranges to create large droplet radii. The parameters describing chemical reaction rates can vary widely depending on concentration levels and specific reactions considered[16]. The reaction rates $k_\pm$ and $\nu_\pm$ are related to elasticity coefficients[17] for which only very few measured values have been reported. Instead of specifying $k_\pm$ and $\nu_\pm$ directly, we therefore choose experimentally relevant turnover times[11] t_R and length-scales $l_\pm$ that are larger than resulting droplet radii such that the droplets are approximately homogeneous. The remaining parameters ($\beta_\pm$, $\nu_\pm$, and $k_\pm$) can be determined using the expressions given in the first column of the Table. The supersaturation ϵ_{div} at which the stationary radius $\bar{R}_s$ becomes unstable, $\mu_{12} = 0$, is obtained by linear stability analysis.

V. REACTION RATES WITH BROKEN DETAILED BALANCE

In our models, chemical reaction rates and diffusion fluxes are maintained in a non-equilibrium steady state. They are driven by the free energy supplied by the chemical potential difference of a higher energy chemical fuel C and a lower energy waste product C', which are maintained by external reservoirs. We illustrate these non-equilibrium conditions in a simple model based on four components A, B, C, C' in a system that exhibits phase separation of the two components A and B.

The chemical potentials of components $n = A, B, C, C'$ can be expressed as

$$\mu_n = k_{\rm B}T \ln(v_n c_n) + w_n \quad , \tag{S.62}$$

where v_n denote molecular volumes. The first term describes the entropy of molecular rearrangements. The contribution w_n captures internal free energies of molecules as well as effects of interactions between molecules[2]. Therefore, w_n depends on composition. For simplicity, we only consider here the dependence on the concentrations of A and B, $w_n(c_A, c_B)$. For a phase-separated system at thermodynamic equilibrium, the chemical potentials of all components n are equal in both phases,

$$\mu_n^+ = \mu_n^- \ , \tag{S.63}$$

where "+" and "-" refer to the phases outside and inside the droplet, respectively. Because of the dependence of w_n on c_A and c_B, the concentrations of all molecular species differ in both phases, $c_n^+ \neq c_n^-$, with

$$\frac{c_n^+}{c_n^-} = \exp\left(\frac{w_n^- - w_n^+}{k_{\rm B}T}\right) \ . \tag{S.64}$$

This difference implies that molecules of a given species typically have a higher affinity to one phase as compared to the other as a result of interactions with other molecules.

The case of a B-rich droplet at equilibrium (without chemical reactions) is illustrated in Fig. S5. Here we consider the case where the concentrations c_C and $c_{C'}$ are higher outside the droplet than inside, corresponding to a smaller affinity to the droplet phase.

We choose a system where the chemical potential μ_B is larger than μ_A, such that $\Delta\mu^{(1)} = \mu_B - \mu_A > 0$, and where the chemical potential μ_C is large enough that $\Delta\mu^{(2)} = \mu_B - \mu_A - \mu_C + \mu_{C'} < 0$, see Fig. S5 B. Note that the value of μ_C can be set by varying the concentration in the external reservoir.

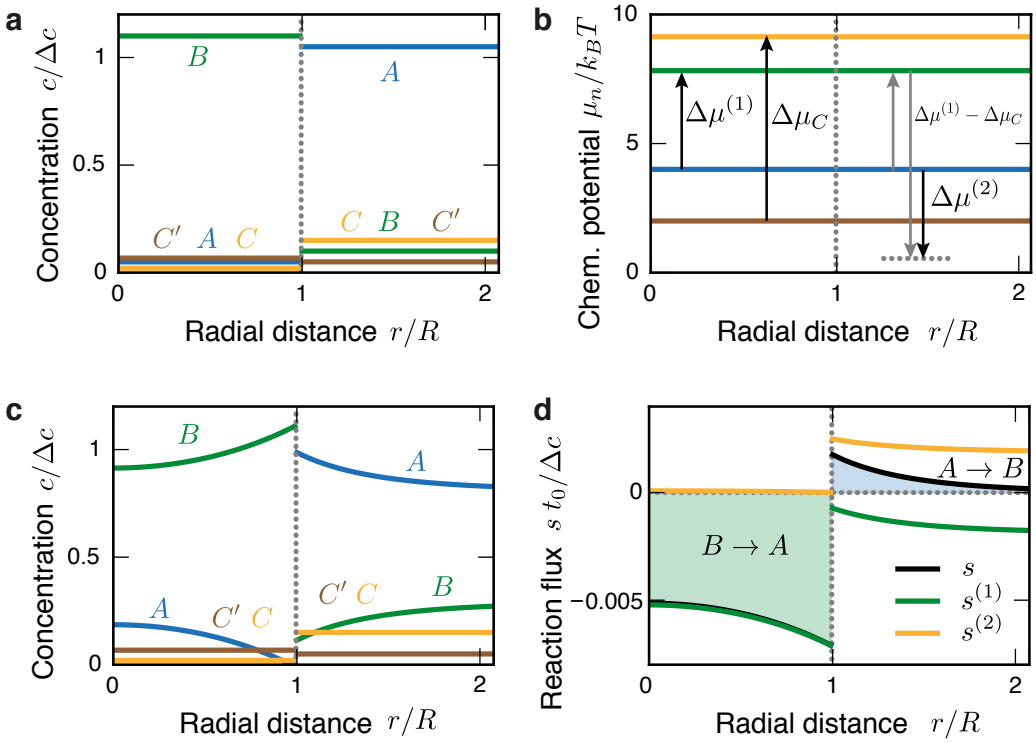

FIG. S5. Concentration profiles and reaction rates in a four-component model including fuel and waste. Radial profiles of concentrations (A) and chemical potentials (B) of molecular species A, B, C and C' for an equilibrium droplet without chemical reactions. The differences in chemical potentials $\Delta\mu^{(1)}$ and $\Delta\mu^{(2)}$ can drive chemical reactions. In the presence of chemical reactions, radial concentration profiles change slightly (C). The corresponding reaction fluxes are shown in (D). The active droplet shown in (C) correspond to the stationary unstable spherical droplet shown in Fig. 1C of the main text which undergoes a division. Parameter values for (A) and (B) are $c_-^{(0)}/\Delta c = 1.1$, $c_+^{(0)}/\Delta c = 0.1$, $v_A\Delta c = 0.87$, $c_C^+/\Delta c = 0.15$, $c_{C'}^+/\Delta c = 0.05$, $(w_C^- - w_C^+)/k_BT = 2$, $(w_{C'}^- - w_{C'}^+)/k_BT = -0.3$, $\Delta w_+^{(1)}/k_BT = -6.17$, and $\Delta w_+^{(2)}/k_BT = 0.135$. In (C) and (D) the same parameters are used together with the reaction parameters $k^{(1)}t_0 = 0.0065$, $k^{(2)}t_0\Delta c = 0.017$, $\epsilon_\pm^{(1)} = 0$, and $\epsilon_\pm^{(2)} = 0$. See Table S1 for the definitions of the time scale t_0 and the concentrations Δc that are used for normalization.

The system can be driven away from equilibrium by the chemical reactions (1) and (2), which are driven by the chemical potential differences $\Delta\mu^{(1)}$ and $\Delta\mu^{(2)}$. The flux of the reaction (1), $B \rightleftharpoons A$, can be written as (see Methods section in the main text)

$$s^{(1)} = s_\leftarrow^{(1)} \left[\exp\left(-\frac{\Delta\mu^{(1)}}{k_BT} \right) - 1 \right] \quad , \tag{S.65}$$

which obeys a local detailed balance condition. Here, the reaction amplitude $s_\leftarrow^{(1)}$ is in general

concentration dependent. Similarly, for the reaction (2), $A + C \rightleftharpoons B + C'$, the reaction flux is

$$s^{(2)} = s^{(2)}_{\rightarrow} \left[1 - \exp\left(\frac{\Delta\mu^{(2)}}{k_{\mathrm{B}}T} \right) \right] \quad . \tag{S.66}$$

Considering these expressions, we find for the situation illustrated in Fig. S5 B that $s^{(1)} < 0$ and $s^{(2)} > 0$ in both phases, so that reaction (1) produces A molecules, while reaction (2) produces B molecules, both inside and outside the droplet. However, the reaction amplitudes $s^{(1)}_{\leftarrow}$ and $s^{(2)}_{\rightarrow}$ can vary strongly with concentration and therefore the magnitudes of the fluxes $s^{(1)}$ and $s^{(2)}$ differ inside and outside the droplet, see Fig. S5 C. The total reaction flux

$$s = s^{(1)} + s^{(2)} \tag{S.67}$$

does not obey a local detailed balance condition. The sign of s depends not only on the chemical potential differences, but also on the reaction amplitudes $s^{(1)}_{\leftarrow}$ and $s^{(2)}_{\rightarrow}$, which depend on local concentrations. For example, the reaction amplitude $s^{(1)}_{\leftarrow}$ is in general a function of concentrations. For vanishing concentration of B, reaction (1) cannot proceed in backward direction and $s^{(1)}_{\leftarrow} = 0$. we therefore write $s^{(1)}_{\leftarrow} = c_B f(c_A, c_B, c_C, c_{C'})$. In the simplest case f is constant. We thus consider

$$s^{(1)}_{\leftarrow} \approx c_B k^{(1)} \ , \tag{S.68}$$

where $k^{(1)}$ is a concentration-independent reaction constant. Using a similar argument for reaction (2), we consider

$$s^{(2)}_{\rightarrow} \approx c_C \ c_A \cdot k^{(2)} \ , \tag{S.69}$$

with reaction constant $k^{(2)}$.

We can now discuss a typical scenario that corresponds to production of A molecules inside the droplet and production of B molecules outside (see Fig. S5 and Methods section in the main text). The amplitude $s^{(2)}_{\rightarrow}$ is smaller inside the droplet where the concentrations c_C and c_A are small, as compared to outside. Furthermore $s^{(1)}_{\leftarrow}$ is smaller outside the droplet, where the concentration c_B is small compared to inside. The total reaction flux s then is typically negative inside the droplet and positive outside (see Figs. 4 and S5).

We can relate this detailed description of the chemical reactions to the simplified representation of the chemical reactions given in Eq. (S.5). First, using (S.65) and (S.66), we have

$$s^{(1)} \simeq k^{(1)} \left(c_A \exp\left[\frac{w_A - w_B}{k_{\mathrm{B}}T} \right] - c_B \right) \tag{S.70}$$

and

$$s^{(2)} \simeq k^{(2)} \left(c_C c_A - c_{C'} c_B \exp\left[\frac{w_B - w_A - w_C + w_{C'}}{k_\mathrm{B} T} \right] \right) , \tag{S.71}$$

where we have considered the simple case where molecular volumes do not change during chemical reactions, $v_A = v_B$ and $v_C = v_{C'}$.

We neglect for simplicity the contributions of the molecules C and C' to the total volume,

$$c_A \simeq \frac{1}{v_A} - c_B \, . \tag{S.72}$$

The concentration c in Eq. (S.5) is $c = c_B$, and the variables $c_\pm^{(0)}$ in Eq. (S.1) correspond to the equilibrium concentrations $c_B^\pm$ of B molecules inside and outside the interface. We can now identify

$$\begin{aligned} \nu_\pm = \pm k^{(1)} & \left[\left(\frac{1}{v_A} - c_\pm^{(0)} \right) \exp\left[\frac{w_A^\pm - w_B^\pm}{k_\mathrm{B} T} \right] - c_\pm^{(0)} \right] \\ & \pm k^{(2)} \left[c_C^\pm \left(\frac{1}{v_A} - c_\pm^{(0)} \right) - c_{C'}^\pm c_\pm^{(0)} \exp\left[\frac{w_B^\pm - w_A^\pm - w_C^\pm + w_{C'}^\pm}{k_\mathrm{B} T} \right] \right] \end{aligned} \tag{S.73}$$

and

$$\begin{aligned} k_\pm = {} & k^{(1)} \left[\exp\left[\frac{w_A^\pm - w_B^\pm}{k_\mathrm{B} T} \right] + 1 \right] + k^{(2)} \left[c_C^\pm + c_{C'}^\pm \exp\left[\frac{w_B^\pm - w_A^\pm - w_C^\pm + w_{C'}^\pm}{k_\mathrm{B} T} \right] \right] \\ & - k^{(1)} \left(\frac{1}{v_A} - c_\pm^{(0)} \right) \exp\left[\frac{w_A^\pm - w_B^\pm}{k_\mathrm{B} T} \right] \frac{1}{k_\mathrm{B} T} \left. \frac{\mathrm{d}(w_A - w_B)}{\mathrm{d}c} \right|_{c_\pm^{(0)}} \\ & + k^{(2)} c_{C'}^\pm c_\pm^{(0)} \exp\left[\frac{w_B^\pm - w_A^\pm - w_C^\pm + w_{C'}^\pm}{k_\mathrm{B} T} \right] \frac{1}{k_\mathrm{B} T} \left. \frac{\mathrm{d}(w_B - w_A - w_C + w_{C'})}{\mathrm{d}c} \right|_{c_\pm^{(0)}} . \end{aligned} \tag{S.74}$$

These expressions show that the parameters $\nu_\pm$ and $k_\pm$ depend explicitly on the fuel concentration c_C and the concentration $c_{C'}$ of the waste product. Furthermore, they depend on molecular interactions described by the energies $w_n^\pm$.

Thus, the active droplet system defined in the Methods section in the main text results from the more detailed model of chemical reactions described here. The dimensionless parameters that need to be specified are: $c_-^{(0)}/\Delta c$, $c_+^{(0)}/\Delta c$, $v_A \Delta c$, $c_C^+/\Delta c$, $c_{C'}^+/\Delta c$, $\exp[(w_C^- - w_C^+)/k_\mathrm{B}T]$, $\exp[(w_{C'}^- - w_{C'}^+)/k_\mathrm{B}T]$, $\exp[\Delta w_+^{(1)}/k_\mathrm{B}T]$, $\exp[\Delta w_+^{(2)}/k_\mathrm{B}T]$, $k^{(1)} t_0$, $k^{(2)} t_0 \Delta c$, and $\epsilon_\pm^{(1)}$, $\epsilon_\pm^{(2)}$, and we consider for simplicity the limit of large diffusion coefficients of C and C', for which c_C and $c_{C'}$ are constant inside and outside of the droplet. Here, we denoted internal energy differences of reactions (1) and (2) as $\Delta w_\pm^{(1)} = w_A^\pm - w_B^\pm$, $\Delta w_\pm^{(2)} = w_B^\pm - w_A^\pm - w_C^\pm + w_{C'}^\pm$, and derivatives of the internal energy with respect to the concentration of B as $\epsilon_\pm^{(1)} = \frac{\Delta c}{k_\mathrm{B}T} \left. \frac{\mathrm{d}(w_A - w_B)}{\mathrm{d}c} \right|_{c_\pm^{(0)}}$ and $\epsilon_\pm^{(2)} =$

$\frac{\Delta c}{k_{\mathrm{B}}T}\left.\frac{\mathrm{d}(w_B - w_A - w_C + w_{C'})}{\mathrm{d}c}\right|_{c_\pm^{(0)}}$. We can calculate the concentrations c_C^-, $c_{C'}^-$ and c_A using Eq. (S.64) and Eq. (S.72). Thus the simplified models of chemical reactions discussed in the main text can be related to a more detailed description of the reactions including explicit concentrations of fuel and waste. An example of a stationary droplet is shown in Fig. S5.

[1] Desai, R. C. & Kapral, R. *Dynamics of Self-organized and Self-assembled Structures* (Cambridge University Press, 2009).

[2] Cahn, J. W. & Hilliard, J. E. Free Energy of a Nonuniform System. I. Interfacial Free Energy. *J. Chem. Phys.* **28**, 258–267 (1958).

[3] Glotzer, S. C., Stauffer, D. & Jan, N. Monte Carlo simulations of phase separation in chemically reactive binary mixtures. *Phys. Rev. Lett.* **72**, 4109–4112 (1994).

[4] Christensen, J. J., Elder, K. & Fogedby, H. C. Phase segregation dynamics of a chemically reactive binary mixture. *Phys. Rev. E* **54**, R2212–R2215 (1996).

[5] Dennis, G. R., Hope, J. J. & Johnsson, M. T. XMDS2: Fast, scalable simulation of coupled stochastic partial differential equations. *Comput. Phys. Commun.* **184**, 201–208 (2013).

[6] Bray, A. Theory of phase-ordering kinetics. *Adv. Phys.* **43**, 357–459 (1994).

[7] Zwicker, D., Hyman, A. A. & Jülicher, F. Suppression of Ostwald ripening in Active Emulsions. *Phys. Rev. E* **92**, 012317 (2015).

[8] Zhong-can, O.-Y. & Helfrich, W. Instability and deformation of a spherical vesicle by pressure. *Phys. Rev. Lett.* **59**, 2486–2488 (1987).

[9] Mullins, W. W. & Sekerka, R. F. Morphological stability of a particle growing by diffusion or heat flow. *J. Appl. Phys.* **34**, 323–329 (1963).

[10] Davis, S. H. *Theory of solidification* (Cambridge University Press, 2001).

[11] Brangwynne, C. P. *et al.* Germline P Granules Are Liquid Droplets That Localize by Controlled Dissolution/Condensation. *Science* **324**, 1729–1732 (2009).

[12] Li, P. *et al.* Phase transitions in the assembly of multivalent signalling proteins. *Nature* **483**, 336–340 (2012).

[13] Safran, S. A. *Statistical thermodynamics of surfaces, interfaces, and membranes*, vol. 90 (Perseus Books, 1994).

[14] Peters, F. & Arabali, D. Interfacial tension between oil and water measured with a modified contour method. *Colloids and Surfaces A: Physicochemical and Engineering Aspects* **426**, 1–5 (2013).

[15] Page, C. A., Bonner, J. S., Sumner, P. L. & Autenrieth, R. L. Solubility of petroleum hydrocarbons in oil/water systems. *Marine Chemistry* **70**, 79 – 87 (2000).

[16] Atkins, P. & de Paula, J. *Atkins' Physical Chemistry* (OUP Oxford, 2010).

[17] Kacser, H., & Burns, J. The control of flux. In *Symp. Soc. Exp. Biol.*, vol. 27, 65–104 (1973).